

FINITE ELEMENT MODEL VALIDATION AND LONG-TERM MONITORING OF CONCRETE ARCH DAMS USING AMBIENT VIBRATION MONITORING

Report to the
Water Research Commission

by

Pilate Moyo¹, Patrick Bukenya¹ & Chris Oosthuizen²

¹University of Cape Town

²Department of Water and Sanitation

Report Number 2244/1/16
ISBN 978-1-4312-0780-0

April 2016

Obtainable from

Water Research Commission
Private Bag X03
GEZINA, 0031

orders@wrc.org.za or download from www.wrc.org.za

DISCLAIMER

This report has been reviewed by the Water Research Commission (WRC) and approved for publication. Approval does not signify that the contents necessarily reflect the views and policies of the WRC nor does mention of trade names or commercial products constitute endorsement or recommendation for use.

EXECUTIVE SUMMARY

Background

Dam safety is concerned with ensuring that the structural integrity of a dam is maintained throughout its service life. This requires a sound understanding of the loading environment, structural behaviour, material deterioration mechanisms and structural performance of a dam at any given time. The most common approaches for dam safety evaluation are visual inspections, instrumented monitoring and finite element modelling. The work presented in this report follows from previous work carried by the authors (Moyo & Oosthuizen, 2013) which focused on demonstrating the application of ambient vibration measurements for structural health monitoring and finite element model validation and updating of concrete arch dams. A unique feature of this project is the integration of continuous ambient vibration monitoring (AVM) and static monitoring of a concrete arch dam. By developing relationships between the dam's response (natural frequencies and dam wall deformations) and the operating loading (reservoir level, temperature) the onset of anomalous behaviour can be detected and the future response of a dam can be predicted.

Key objectives

Moyo & Oosthuizen (2013) demonstrated that AVM is a viable methodology for tracking the behaviour of arch dams. In particular, it was shown that natural frequencies are sensitive to changes in the water level. Finite element models showed that seasonal temperature variations had minimal influence on the natural frequencies of arch dams. However this was not validated by field measurements. Moyo & Oosthuizen (2013) also showed that the Westergaard method for hydrodynamic analysis of dams over estimates the added non-structural mass on the dam wall due to the reservoir. It is not clear if the overestimation is due to the shape of the reservoir or inherent in the Westergaard method itself. Thus the two main objectives of the current project were;

- i) Investigate the effect of reservoir orientation on the dynamic properties of arch dams using fluid-structure interaction approach. This method is more accurate compared to the Westergaard approach.
- ii) Evaluate the accuracy of the Westergaard method for ambient vibration analysis of arch dams.

- iii) Investigate the relationship between dam behaviour (natural frequencies and static deformations) and the loading (seasonal temperature variation and water level).

Methodology

Roode Elsberg Dam, a double curvature arch dam, was used as a case study in the investigations.

Numerical investigations using the Westergaard method and the fluid structure interaction were carried out in finite element analysis package, ABAQUS, and the results of the investigations were compared to field measurements.

Multiple regression analysis was used to investigate the relationship between the loading and response of the dam.

Findings

The investigations revealed that;

- i) Natural frequencies of arch dams are not very sensitive to reservoir orientation.
- ii) A comparison of the results of hydrodynamic analysis of the dam, show that the natural frequencies obtained using the Westergaard method are about 23% lower than the natural frequencies obtained using the fluid structure interaction approach.
- iii) Natural frequencies obtained using the Westergaard method are approximately 20% lower than measured natural frequencies, while the results fluid structure interaction approach are within 3% of measured natural frequencies.
- iv) The dynamic behaviour of arch dams is strongly dependent on the reservoir level. The natural frequencies of the dam decrease with water level. The dam's dynamic behaviour is weakly influenced by seasonal temperature variation.
- v) The seasonal deformation of the dam is strongly dependent on temperature variation. While the seasonal variation of deformations is largely driven by temperature variation, the reservoir level does influence the deformation of the dam especially as the dam fills rapidly. This is an important observation which has only been possible through continuous monitoring of both static deformations and natural frequencies of the dam.

Based on the results of this study it can be concluded that;

- i) The Westergaard method over-estimates the added mass for dynamic analysis of arch dams under operating conditions. It must be pointed out that the method was originally developed for the analysis of dams subjected to seismic loading. Thus Westergaard method in its current form is not suitable for dynamic analysis of arch dams under ambient conditions.
- ii) Dynamic monitoring should form part of a dam safety evaluation strategy as it provides information that improves understanding of structural behaviour of dams. The information obtained from dynamic monitoring is critical for finite element model updating.

Recommendations

It is recommended that ambient vibration monitoring should form part of dam surveillance systems. This will enable robust detection of anomalous behaviour of arch dams by minimising false alarms. Ambient vibration monitoring also provides key information for developing realistic finite element models of arch dams.

It is clear that seasonal temperature variations contribute significantly to the deformation behaviour of arch dams. It is also well known that temperature has a strong influence on aggregate-alkali reactions which lead to swelling and deterioration of concrete. Long term temperature shifts due to climate change would thus have an impact on the structural performance of dams. It is recommended to investigate the impacts of climate change on the structural performance concrete arch dams in South Africa.

ACKNOWLEDGEMENTS

The authors acknowledge the financial contribution of the Water Research Commission in the project and the previous project reported in Moyo & Oosthuizen (2013), which forms the basis for present project. The Department of Water and Sanitation has given us access to the dams and this is greatly appreciated. CoMSIRU provides a wonderful research environment and this is acknowledged.

The Reference Group, comprising of the following individuals, are acknowledged for their critical and valuable input throughout the project:

Mr W Nomquphu	:	Water Research Commission (Chair)
Dr Chris Oosthuizen	:	Department of Water and Sanitation
Prof Jan Wium	:	University of Stellenbosch
Mr Piet Naude	:	Private
Prof Mark Alexander	:	University of Cape Town
Dr Sifiso Nhleko	:	South African National Nuclear Regulator
Mr Louis Hattingh	:	Hattingh Anderson Associates CC

TABLE OF CONTENTS

EXECUTIVE SUMMARY	iii
ACKNOWLEDGEMENTS	vi
LIST OF FIGURES	ix
LIST OF TABLES	x
NOMENCLATURE.....	xi
1 Introduction.....	1
1.1 Background	1
1.2 Objectives.....	1
1.3 Limitations and Scope of Project	2
2 Dynamic Analysis of arch dams.....	3
2.1 Introduction	3
2.2 Added mass approach (Westergaard Method)	3
2.3 Fluid Structure Interaction	6
2.4 Summary	8
3 Hydrodynamic modelling of Roode Elsberg dam	9
3.1 Description of Dam	9
3.2 FE Model.....	10
3.2.1 Modelling Arch Dam Wall	10
3.2.2 Modelling the Foundation Part	11
3.2.3 Assembly and Meshing.....	12
3.2.4 Material Properties.....	14
3.3 Fluid structure Interaction Model.....	15
3.3.1 Boundary Conditions, Constraints and Interactions	17
3.4 Westergaard Method	18
3.4.1 Added mass	18
3.4.2 Partitioning of the Dam Wall.....	21
3.4.3 Application of Inertial Mass	21

3.5	Parametric Study of Reservoir Orientation and Geometry	22
3.6	Results and Discussion of hydrodynamic analysis	23
3.6.1	Natural frequencies and mode shapes.....	23
3.6.2	Effect of reservoir geometry on natural frequencies	26
3.6.3	FSI Hydrodynamic Pressure Distribution.....	27
3.7	Summary	29
4	Continuous monitoring of Roode Elsberg dam.....	30
4.1	Introduction	30
4.2	Description of the dynamic monitoring system	30
4.3	Description of Global Navigation Satellite System	30
4.4	Measurement of environmental and operation factors.....	32
4.5	Results and discussions	34
4.5.1	Reservoir Level.....	34
4.5.2	Ambient and reservoir temperatures.....	34
4.5.3	Dynamic response.....	40
4.5.4	Static response	42
4.6	Summary of observations.....	45
5	Statistical modelling.....	46
6	Conclusions & Recommendations.....	52
6.1	Conclusions	52
6.2	Recommendations	53
7	References.....	54

LIST OF FIGURES

Figure 3.1: Roode Elsberg Dam located in Worcester Western Cape, South Africa	9
Figure 3.2: Downstream side of the arch dam (Nzuza, 2013).	11
Figure 3.3: (left) Wire developed feature of foundation and (right) completed solid region of foundation.	12
Figure 3.4: (left) Merging of Dam wall and foundation part. (right) completed merged instance of the two parts (Nzuza, 2013).....	13
Figure 3.5: Completed mesh of dam foundation part using C3D10 tetrahedral elements.....	14
Figure 3.6: (left) Fluid part created using cross sectional wires and (right) lofted continuous fluid part considered to extend three times the dam wall height.	16
Figure 3.7: Meshed fluid region using AC3D10 quadratic tetrahedral elements and dam-foundation part meshed using C3D10 quadratic tetrahedral elements.	16
Figure 3.8: Boundary conditions, constraints and interactions applied to the FSI model	18
Figure 3.9: Dam wall partitioned to allow for application of the Westergaard added masses.	21
Figure 3.10: Element nodes used to apply the added mass as inertial nodal mass.	22
Figure 3.11: Diverging and asymmetric cases considered in the parametric study.....	23
Figure 3.12: Pressure distribution at quarter arc location for Mode 1	28
Figure 3.13: Pressure distribution at crown level for mode 2.....	28
Figure 3.14: Pressure distribution at crown position for mode 3.....	29
Figure 4.1: Accelerometers on the dam crest and data acquisition system in the upper dam gallery	30
Figure 4.2: GPS network on Roode Elsberg dam	31
Figure 4.3: Base station P01 on Roode Elsberg dam.....	32
Figure 4.4: Staff gauges for water level measurements	33
Figure 4.5: Weather station installed on the dam crest near the spillway.....	33
Figure 4.6: Water level	34
Figure 4.7: Ambient and reservoir temperature variation.....	36
Figure 4.8: Reservoir temperature variation	37
Figure 4.9: Smoothed temperature variation	38
Figure 4.10: Smoothed temperature variation	39
Figure 4.11: Singular values of spectral densities from observed data.....	40
Figure 4.12: Sample Stabilization diagram.....	40
Figure 4.13: Variation of mode 1 with time	41
Figure 4.14: Variation of mode 2 with time	41
Figure 4.15: Variation of mode 3 with time	42

Figure 4.16: Variation of mode 1 and water level with time	42
Figure 4.17: Normalised displacements in the radial direction	43
Figure 4.18: Normalised displacements in the tangential direction.....	43
Figure 4.19: Normalised displacements in the vertical direction	44
Figure 4.20: Normalised displacements in the radial direction and air temperature	44
Figure 4.21: Normalised displacements in the radial direction and water level.....	45
Figure 5.1: Water level versus mode 1	46
Figure 5.2: Air temperature vs mode 1	47
Figure 5.3: Normalised radial displacement versus monthly average air temperature.....	47
Figure 5.4: Normalised radial displacement versus monthly average air temperature.....	47
Figure 5.5: MLR-Mode 1.....	50
Figure 5.6: MLR-displacement.....	51

LIST OF TABLES

Table 3.1: Properties of Roode Elsberg Dam	10
Table 3.2: Linear elastic material properties of dam wall and foundation part	15
Table 3.3: Material parameters assigned to the fluid medium.....	16
Table 3.4: Comparison of natural frequencies (Hz) obtained from AVT test in Sep-2013 with the FSI model and Westergaard method.....	24
Table 3.5: Comparison of natural frequencies (Hz) obtained from AVT test in Sep-2013 with the FSI model and Westergaard method.....	24
Table 5.1: Coefficients of linear regression.....	49

NOMENCLATURE

Latin Upper Case

A	Tributary area
E	Strain displacement matrix
C	Damping matrix
\bar{D}	Stress-strain matrix
E_f	Foundation material elastic modulus
E_c	Concrete material elastic modulus
\vec{f}	Vector of nodal force
F_p	Ambient hydrodynamic forces
F_g	Forces induced by ground motion
G	Lame's constant
G_{xx}	Value of cross spectrum between signal and frequency
H	Depth of reservoir
K	Bulk Modulus
K_s	Stiffness matrix
L	Dam reservoir length
M_s	Mass of Solid
M_f	Mass of fluid
N	Array of shape functions
P	Hydrodynamic pressure
Q	Transformation matrix of hydrodynamic pressures into forces
R	Residual of Galerkin FEM
R_f	Foundation radius

S_{fs}	Coupling of the solid and acoustic motion
U	The unitary matrix holding singular values
X^L	Matrix of left eigenvector
X^R	Matrix of right eigenvector
Z	Distance from the base of the dam
C_{ijkl}	Rank four material stiffness tensor

Latin Lower Case

c_s	Propagation velocity of p-wave and s-wave
ϵ	Surface emissivity
f	External loads
m	Meters
m_{ai}	Added mass matrix
n	Maximum number of time steps
n_s	Outward normal direction from reservoir surface
p	Hydrodynamic pressure in the fluid
r_h	Relative humidity
s	Seconds
t	Time
\ddot{u}	Acceleration
\ddot{u}_g	Horizontal ground acceleration
\dot{u}	Velocity
u	Displacement
w	Test / weighting function

x, y, z Cartesian coordinate system

y Reservoir depth

z Foundation depth

Greek Upper Case

∂ Partial differential

Γ_{α}^L Left acoustic participation factor

Γ_{α}^R Right acoustic participation factor

∇^2 Laplacian operator

Δt Time step length

Ω Finite element domain

Greek lower Case

α Westergaard pressure distribution

β Sloping angle of dam surface

δ Variational field

ρ Unit mass of water

θ_p Angle of parabolic section of the dam wall

θ_R Angle of radial section of the dam wall

λ Normal direction cosines

ϕ Matrix of mode shapes

φ Latitude of location

ω Angular frequency

ϵ_{kl}^s	Strain tensor
$\bar{\sigma}$	Average stress values
γ_{xy}	Coherence function

1 INTRODUCTION

1.1 Background

In our earlier study (Moyo & Oosthuizen, 2013) it was observed that the Westergaard method overestimates the added mass for dynamic analysis of concrete arch dams leading to estimated natural frequencies lower than measured frequencies under ambient conditions. The dam's response and internal forces estimated from such a model would therefore be higher than actual responses and internal forces experienced by the dam. The present work seeks to minimise the discrepancy between measured dynamic properties and the finite element models. The main challenge to address is the distribution of the mass of water that participates in the dynamic behaviour of the dam under ambient conditions. In particular the effect of the orientation of the reservoir on the distribution of the active mass will be investigated. This will be followed by a comparative study to quantify the differences between the Westergaard method, the fluid interaction approach and measured data. This will lead to more realistic analysis of arch dams using the Westergaard method.

Moyo & Oosthuizen (2013) demonstrated the suitability of ambient vibration monitoring of arch for structural health monitoring. A continuous ambient vibration monitoring system has been installed on Roode Elsberg as part of the existing structural monitoring and surveillance on the dam. The results of ambient vibration monitoring are reported and integrated with static monitoring using multivariate statistics.

1.2 Objectives

The aim of this research is to develop an updatable dynamic finite element model of the Roode Elsberg arch dam based on ambient vibration testing.

The objectives of this research are outlined as follows:

1. To investigate the effect of a reservoir's orientation and geometry on the dynamic properties of the dam.
2. To analyse and assess the discrepancies in modal parameters produced by the Modified Westergaard and Fluid Structure Interaction (FSI) analysis methods.

3. To develop a dynamic updatable finite element model (FEM) of the Roode Elsberg concrete arch dam.
4. To conduct ambient vibration tests on the Roode Elsberg dam, measuring the operational dynamic properties, and hence, validate the dynamic updatable finite element model of the dam
5. Develop an integrated anomaly detection procedure based on static and dynamic measurements.

1.3 Limitations and Scope of Project

The scope of the research is limited to the Roode Elsberg dam located in Worcester, Western Cape, South Africa. Research work conducted in this project is aimed towards developing a Finite Element Model (FEM), which will be used to monitor and assess the safety of the dam. An existing static finite element model of the Roode Elsberg dam has been verified and will form basis of the dynamic model. The research was limited to the following:

1. The study focuses only on the approach of modelling the hydrodynamic loading acting on the dam. Development of sedimentation and existing crack defects on the dam are not included in this work. The previously stated could have a significant influence on the final model.
2. There is inadequate data for the elastic properties of the foundation for Roode Elsberg Dam. The left and right abutments of the valley including the bedrock beneath the dam have dissimilar elastic properties.
3. The operational dynamic properties obtained for the dam were extracted from ambient vibration measurements carried out on the dam.

2 DYNAMIC ANALYSIS OF ARCH DAMS

2.1 Introduction

Two aspects of dynamic analysis are critical for dam safety management. Firstly, dynamic analysis is carried out seismic safety evaluation of dams in earthquake prone areas. Secondly, the dynamic properties of dams (mode shapes and natural frequencies) are system parameters and can be used for monitoring the structural behaviour of dams. In the case of structural monitoring, dynamic properties are used for detecting deviations from normal behaviour. The challenge with dynamic analysis of arch dams is estimating the hydrodynamic pressure and thus mass of reservoir water that contributes to dynamic response of dams under earthquake loads. The most commonly used techniques for dynamic analysis of arch dams are the added mass approach and the fluid structure interaction approach. This section provides a brief summary of these methods techniques, highlighting the advantages and disadvantages.

2.2 Added mass approach (Westergaard Method)

Westergaard (1933) proposed the added mass approach, commonly referred to as the Westergaard method, for estimating hydrodynamic pressure on the upstream face of a dam wall during an earthquake. The most generalised form of the Westergaard method (Kou, 1982) assumes a parabolic variation of hydrodynamic pressure on the upstream face of a dam (Figure 2.1), with the pressure at any node i , given by:

$$p_i = \alpha_i \ddot{u}_{ni} \quad (2.1)$$

Where:

$$\alpha_i = \frac{7}{8} \rho_w \sqrt{H_i(H_i - Z_i)} \quad (2.2)$$

p_i = hydrodynamic pressure at node i .

α_i = Westergaard pressure coefficient

\ddot{u}_{ni} = total normal acceleration at node i

ρ_w = mass density of water

H_i = depth of water at a vertical section that includes node i .

Z_i – the height of node i above the base of the dam

The normal acceleration \ddot{u}_{ni} , can be expressed in terms of Cartesian coordinate components of ground acceleration and components of acceleration of node i relative to the base of the dam using direction normals as follows;

$$\ddot{u}_{ni} = \lambda_i (\ddot{u} + \beta \ddot{u}_g) \quad (2.3)$$

$\lambda_i = [\lambda_{xi}, \lambda_{yi}, \lambda_{zi}]$ = vector of direction cosines at node i ,

β influence coefficient matrix representing structural displacements resulting from a unit displacement in each component of the support motions

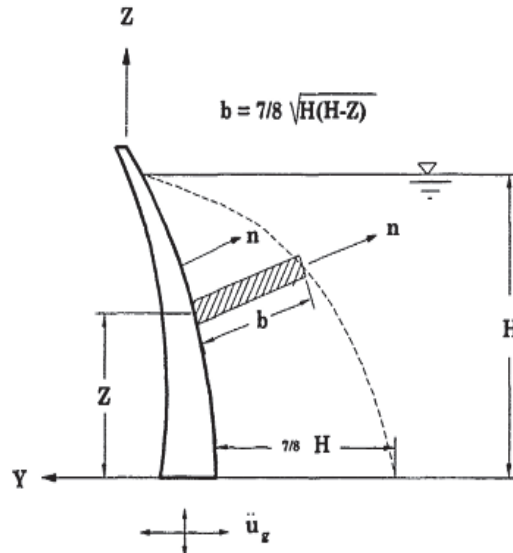


Figure 2.1: Body of water acting normally to the dam surface. (Kuo, 1982)

A simple method to obtain nodal loads, is to lump the hydrodynamic pressures by multiplying by the tributary area associated with that node. The hydrodynamic pressure is assumed to be constant over the tributary area and has the same value as node i , and is defined to act normal to the surface

of the dam at that point. Since the pressures act normal on the surface the same could be said about the nodal forces defined in equation 2.4.

$$F_{ni} = -p_i A_i \quad (2.4)$$

Where

F_{ni} = Equivalent normal hydrodynamic nodal force, outward normal from the dam face as positive

A_i = tributary area associated with node i

The normal force can be resolved into its Cartesian components which are given by equation 2.5.

$$F_i = F_{ni} \lambda_i^T \quad (2.5)$$

Where

$$F_i = [F_x, F_y, F_z]$$

Combining equations 2.1 and 2.4 with 2.5 leads to equation 2.6.

$$F_i = -m_{ai}(\ddot{u} + \beta \ddot{u}_g) \quad (2.6)$$

Where:

$$m_{ai} = \alpha A_i \lambda_i^T \lambda_i \quad (2.7)$$

Here m_{ai} is the added mass matrix as a result of the hydrodynamic forces acting on the upstream surface of the dam wall. The added mass matrix is a 3x3 sub-matrix associated with each node, which is not coupled with the neighbouring node. The added mass sub-matrices are substituted into the equation of motion (equation 2.8) to include the hydrodynamic effects of the reservoir (Ghanaat, 1993).

$$[m + m_a]\{\ddot{u}\} + [c]\{\dot{u}\} + [k]\{u\} = -[m + m_a](\beta \ddot{u}_g) \quad (2.8)$$

The right hand side of equation 2.8 is the effective earthquake load which is dependent on the added mass of the reservoir and the as well as the mass of the dam structure. The added mass of the reservoir needs to be combined directly with the mass matrix of the upstream dam wall surface when implementing the Westergaard added mass method. For each node the mass of the concrete associated with that element is combined with added mass of the impounded water.

2.3 Fluid Structure Interaction

The Westergaard added mass method is computationally efficient and simple to implement in finite element analysis, but does not provide a good representation of the hydrodynamic forces exerted on concrete dams. An alternative approach that offers better idealisation of hydrodynamic pressure on the up-stream surface of dams subjected to seismic events is the fluid structure interaction approach. In this approach hydrodynamic pressures are assumed to be governed by the wave equation (equation 2.9). The solution for the resulting coupled system requires modelling procedures that account for both fluid and solid domains (Figure 2.2). This is achieved through equation 2.10 (Tillioune & Seghir, 1998), with displacements of the dam wall u and pressures p of the fluid as the arguments of the system.

$$\nabla^2 p = 0 \quad (2.9)$$

Where

∇^2 = Laplacian operator in three dimensions

$p(x,y,z,t)$ = Hydrodynamic pressure in excess of the static pressure in the fluid domain Ω (Figure 2.2).

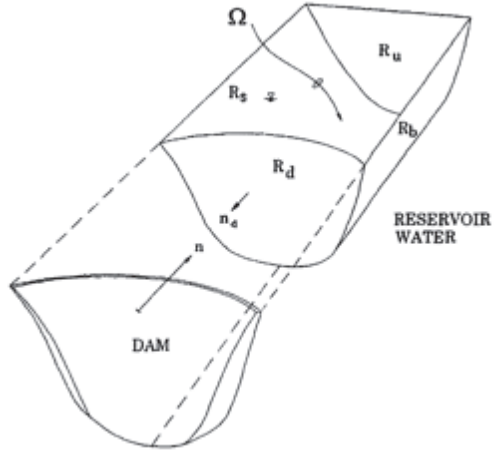


Figure 2.2: Dam and reservoir water domains (Ghanaat, 1993)

$$\begin{bmatrix} m & 0 \\ \rho_w Q^T & m_a \end{bmatrix} \begin{bmatrix} \ddot{u} \\ \ddot{p} \end{bmatrix} + \begin{bmatrix} c & 0 \\ 0 & c_a \end{bmatrix} \begin{bmatrix} \dot{u} \\ \dot{p} \end{bmatrix} + \begin{bmatrix} k & 0 \\ 0 & k_a \end{bmatrix} \begin{bmatrix} u \\ p \end{bmatrix} = \begin{bmatrix} F_G \\ 0 \end{bmatrix} \quad (2.10)$$

Where

m = Dam wall-foundation system mass matrix

m_a = Impounded fluid mass matrix

c = Dam wall-foundation system damping coefficient matrix

c_a = Impounded fluid damping coefficient matrix

k = dam-foundation system stiffness matrix

k_a – Impounded fluid bulk modulus matrix

Q = Transformation matrix that converts nodal pressures into hydrodynamic forces

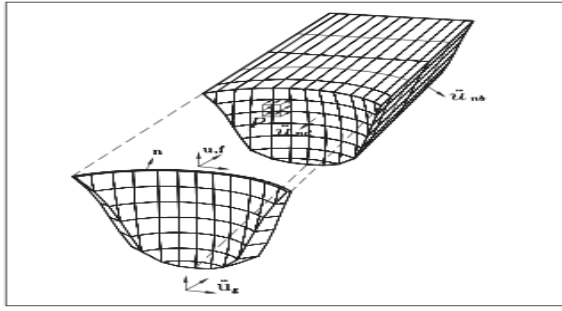


Figure 2.3: discretisation of dam wall and compressible impounded water body (Ghanaat, 1993)

It should be pointed out that in equation 2.10, the fluid is assumed to be compressible. The idea of water compressibility in the analysis of seismic loading induced hydrodynamic effects was first introduced by Fok and Chopra (1985). They introduced frequency-dependent hydrodynamic terms in the equation of motion which could be interpreted as an added mass, added damping and added force. The added damping term is as a result of the refraction of hydrodynamic pressure waves into the absorptive reservoir bottom and propagation of pressure waves in the upstream direction (Figure 2.3). The energy loss is approximated by the wave reflective coefficient α , defined as the ratio of reflected-to-incident wave amplitude of a pressure wave striking the reservoir bottom (US Army Corps of Engineers, 1994). The value of α can be varied from 1 for a rigid nonabsorptive boundary and $\alpha = 0$ for a fully absorptive boundary.

2.4 Summary

Equations 2.8 and 2.10 can be used to obtain the dynamic response of arch dams (displacements and internal forces) as well as the modal parameters (mode shapes and natural frequencies) using finite element and finite volume methods. The accuracy of the solutions is largely dependent on how well each technique estimates the mass of the reservoir water that contributes to the dynamic response during an earthquake in the case of response analysis or the mass of water that contributes to the free vibration response of a dam under normal operating conditions.

3 HYDRODYNAMIC MODELLING OF ROODE ELSBERG DAM

3.1 Description of Dam

Roode Elsberg Dam is a double curvature concrete-arch dam that lies in the Sanddrift River and is located at $33^{\circ}25'39''S$ latitude and $19^{\circ}34'01''E$ longitude which is 30 km away from the town of Worcester, in the Western Cape Province of South Africa. The dam is the lower of two storage dams built in the Sanddrift River to provide supplementary water for 2535 ha of land under irrigation. A concrete lined tunnel, 1.98 m in diameter and 5.2 km long conveys the water from the dam to Hex river valley where distribution is by an enclosed pipe system (Department of Water Affairs, 1971).

The dam was designed to be 72 m in height (from lowest foundation level) with a centrally located uncontrolled over spill and reservoir capacity of 8.21 million m^3 (Figure 3.12).

Roode Elsberg is a double curvature arch dam, which has concentric horizontal arches and parabolic vertical arches constructed from different reference points over its height. The dam was built with a pulvino pad which acts as cushion layer, assisting in distributing the load into the abutments and foundation. The Cape Town Department of Water Affairs states that, since the dam began its operation in 1968, there has been continuous sedimentation occurring at a rate of 4.6%, resulting in a reduction in the volume of water stored (Department of Water Affairs, 1971)



Figure 3.1: Roode Elsberg Dam located in Worcester Western Cape, South Africa

The geometric and material data of Roode Elsberg Dam were sourced from design drawings made available by the Department of Water Affairs (DWA). Table 3.1 provides some of the main characteristics of the dam.

Table 3.1: Properties of Roode Elsberg Dam	
Main Characteristics	Value
Foundation	
Maximum height (m)	72
Foundation altitude (m)	506
Dam body	
Crest altitude (masl)	577
Crest width (m)	2.6
Crest length (m)	274
Spillway length (m)	76
Reservoir	
Normal elevation of water (masl)	573
Minimum elevation of water (masl)	518
Reservoir normal capacity (m^3)	8.21×10^6
Reservoir minimum capacity (m^3)	2.05×10^6

This was carried out by comparing the modal parameters obtained from the two methods. A geometric dam wall was created using the Roode Elsberg dam drawings, where the complex geometry was simplified to not include the pulvino (cushion layer) and made symmetric about the centre line of the uncontrolled spillway. The above dam was chosen as a case study would be conducted to verify the formulations.

3.2 FE Model

3.2.1 Modelling Arch Dam Wall

An existing dam wall system used in the static and temperature analysis (Nzuza 2013) was employed in this dynamic study. The dam was created with the concept of modelling the cantilevered arch blocks and the pulvino cushion as a monolithic system. Roode Elsberg dam is considered to be a complex arch dam due the variation in horizontal and vertical radii. Therefore, the dam wall part was created separately from the foundation using the

lofting feature in ABAQUS. Horizontal reference planes, varying sub-tension angles and arch thicknesses defined in the designing drawings were used to construct the reference datum planes and cross sections of the subtended horizontal arches. This allowed for horizontal closed loop arches constituting the pulvino sub-tensions to be sketched and lofted. Figure 3.2 shows an illustration of the downstream side of the Roode Elsberg dam model.

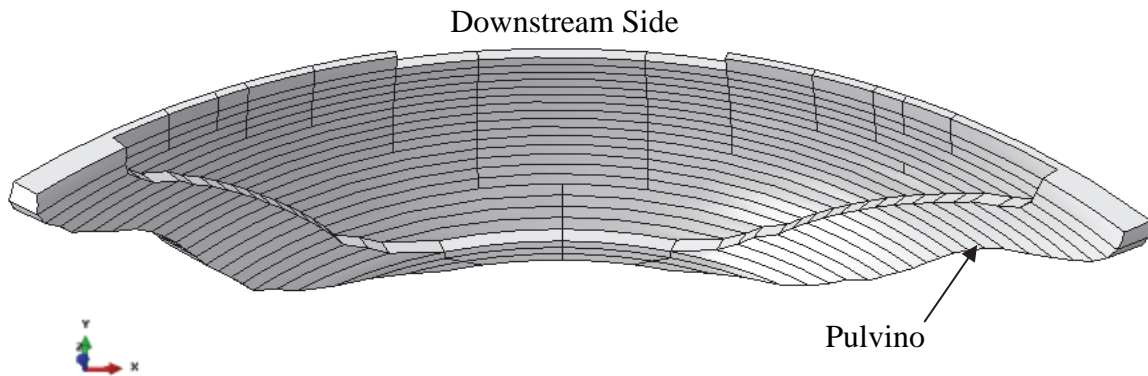


Figure 3.2: Downstream side of the arch dam (Nzuza, 2013).

3.2.2 Modelling the Foundation Part

An idealistic foundation includes all geological features and extends to a distance where boundary effects have no influence on the stresses and dynamic characteristics. This becomes practically impossible as finite element techniques are not yet sufficiently developed, and models would become computationally intensive. The foundation region used in the static analysis was considered to be adequate enough for the dynamic analysis of the dam. The region of the foundation was created using the simplified approach considered in the US Army Corps of Engineers (1994). It specifies that a flexible foundation rock system must be considered, that requires the deformation modulus of the supporting rocks, which accounts for faults and joints in the foundation rock and the Poisson's ratio to be defined for the material properties.

According to jacking field tests conducted on the foundation, it was evident that the left abutment is stiffer than the right abutment. It is not clear where the distinguishing boundary lies, an implicit assumption was made for the modulus of deformation of the foundation system: 25 GPa on the left and bottom sections hard rock-grey region (Figure 3.3), 20 GPa

on the bottom right soft rock – blue region (figure 3.14) and 23 GPa on the top right section soft rock – red (Figure 3.3). Figure 3.3 shows the foundation wire region and the completed lofted solid region.

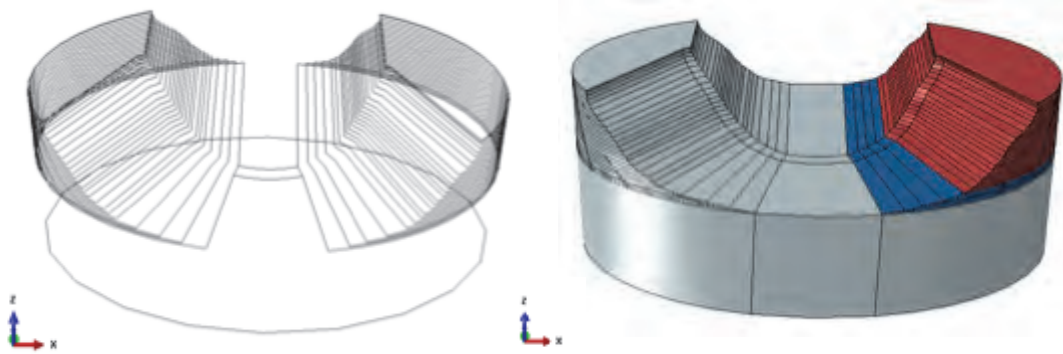


Figure 3.3: (left) Wire developed feature of foundation and (right) completed solid region of foundation.

The foundation walls were created using elliptic planes cut into the supporting canyons, and oriented normally to the dam wall interface. The elliptic planes were created with a major and minor radii of 430 m and 280 m, respectively. The above is in accordance with a radius of two times the height of the dam for flexible foundation rocks (since $E_f \leq 0.5E_c$), which is recommended by the US Army Corps of Engineers (1994). FERC (1999) recommends that the ratio of the foundation depth to the dam wall depth should be in the range of 1.0 to 1.5. The foundation depth was set to extend to a depth 1.5 times the height of the dam, resulting in a foundation of 90 m in depth.

3.2.3 Assembly and Meshing

Two independent native part instances were created for the dam and foundation part in the Assembly module. These were merged into forming a new monolithic part which would allow compatibility of the elements and the mesh at the interface of the concrete wall – foundation rock. The merging still kept the material properties of concrete for the wall and the rock properties for the foundation parts. Figure 3.4 shows the merging of the dam wall part with the truncated massless foundation part.

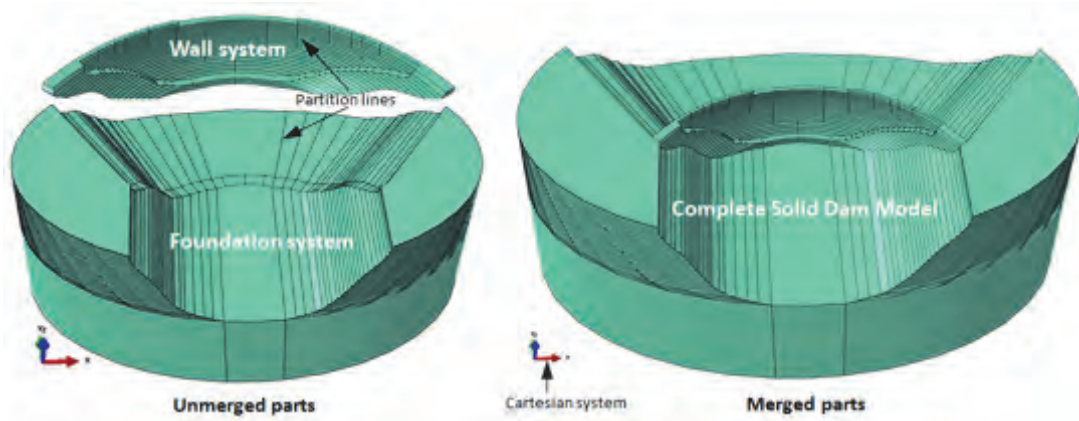


Figure 3.4: (left) Merging of Dam wall and foundation part. (right) completed merged instance of the two parts (Nzuza, 2013).

As previously determined, there is no rule of thumb for meshing arch dams but guidelines do exist stipulating a few conditions to be considered. Three different meshing techniques were considered after the final mesh was chosen. The main factors governing the ideology behind the selection of the final mesh included the size and geometry of the dam, type of elements to be used, type and location of spillway, foundation profile, and the dynamic characteristics of the dam. A meshing scheme that uses quadratic continuum displacement 10-node tetrahedral elements (C3D10) was selected. The wall system was meshed using quadratic tetrahedral C3D10 elements with an approximate global seed size of 7. The mesh was refined to 1612 elements and consisted of 9203 nodes. Due to the complexity of the foundation profile, C3D10 elements also had to be used. These elements are ideal in modelling regions with high degrees of curvature. They also helped in reducing computational time as the element consisted of 10 nodes and resulted in only 50421 elements being used, constituting 67742 nodes. Figure 3.5 shows the completed dam wall-foundation mesh constituting of C3D10 elements.

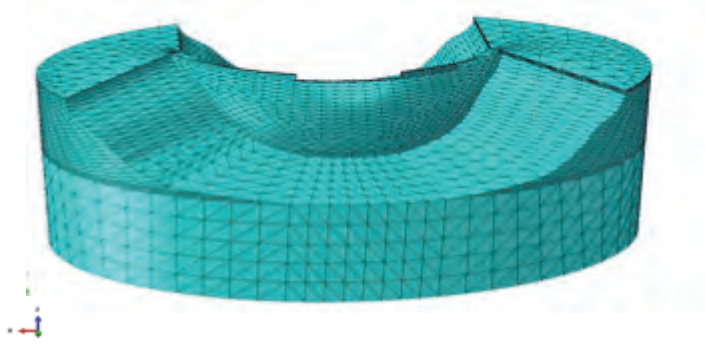


Figure 3.5: Completed mesh of dam foundation part using C3D10 tetrahedral elements

3.2.4 Material Properties

In assigning material properties to the dam, the concrete elastic properties were assumed to be isotropic and homogenous throughout the part. According to the US Army Corps of Engineers (1994) a dynamic study only requires three material properties to be assigned to the dam wall part; these include the dynamic modulus, Poisson's ratio and the unit weight of concrete. The dynamic modulus of concrete is estimated by using empirical methods which require the static modulus to be known. For Roode Elsberg dam the working drawings indicated that the dam wall had a 28 day mean strength of 29 MPa with a standard deviation of 4.1 MPa. With an understanding that concrete properties change with time, the effects of creep had to be taken into account. This was done by correlating to a static modulus (inclusive of creep effects) E'_c of 31 GPa using Fulton's concrete technology (2009). The dynamic modulus of concrete was obtained using the empirical formulation (3.9) accepted in the British testing standard BS8110 part 2. The dynamic modulus of concrete for the dam wall was estimated to be 40 GPa with an assumed standard deviation of 5 GPa as suggested by Fultons (2009).

Where

E'_c = Sustained static young's modulus including effects of creep.

E_d = Dynamic modulus of concrete

$$E'_c = 1.25E_d - 19 \quad (3.1)$$

Summarised in Table 3.5 are the elastic material properties assigned to the arch dam, and the foundation properties assumed for the supporting foundation rock made of Table Mountain quartzitic sandstone as specified in design drawing no. 43938 (Department of Water Affairs, 1971). Linear properties were assigned to the model, as a linear perturbation solver would be used to compute the eigenvalues.

Table 3.2: Linear elastic material properties of dam wall and foundation part

Property and Symbol	SI Units	Concrete Wall	Rock Foundation		
			Left	Bedrock	Right
Modulus of elasticity (E_d)	GPa	44	25	25	23/20
Density (ρ)	$\frac{kg}{m^3}$	2400	-	-	-
Poisson's ratio (ν)	-	0.22	0.25	0.25	0.25

3.3 Fluid structure Interaction Model

Acoustic finite elements were used to provide a realistic representation of the complicated geometry of the impounded water body. The fluid boundary medium was created using the ABAQUS lofting technique. The long sided boundaries were made to coincide geometrically with the foundation profile. This was necessary as the fluid-foundation rock interface would have to be coupled in the later stages. The fluid medium was extended to a length 3 times the height of the Roode Elsberg arch dam (Figure 3.6), and assigned the water material properties.

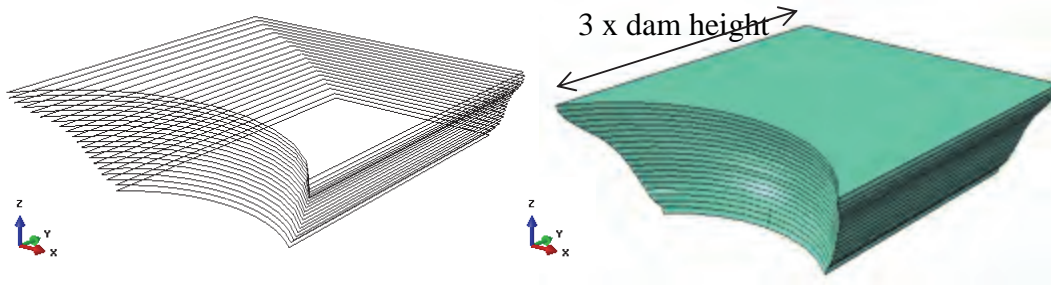


Figure 3.6: (left) Fluid part created using cross sectional wires and (right) lofted continuous fluid part considered to extend three times the dam wall height.

Table 3.3: Material parameters assigned to the fluid medium.

	Fluid Medium
Bulk Modulus (GPa)	2,2
Density ($\frac{kg}{m^3}$)	1000



Figure 3.7: Meshed fluid region using AC3D10 quadratic tetrahedral elements and dam-foundation part meshed using C3D10 quadratic tetrahedral elements.

The fluid was coupled to the dam wall and foundation rock side using the surface based contact tie technique. The dam wall and foundation rock interacting surfaces were assigned the master surface, and the fluid as the slave. The river bed material was not modelled as it did not form part of the investigation, resulting in an opening between the foundation bed

and fluid bottom of approximately 15 meters. The absorption of energy at the supporting foundation rocks and bedrock was not modelled as no geological information was available.

3.3.1 Boundary Conditions, Constraints and Interactions

The boundary condition assigned to the dam wall and the fluid region constituted of the following: (i) The dam-foundation interaction was not considered by applying a completely rigid boundary system, fully restraining the displacement and rotational degrees of freedom on the dam wall perimeter. (ii) The pressure on the fluid surface was considered to be atmospheric and assigned a magnitude of zero. (iii) A surface based tie constraint was used between the upstream dam surface and fluid interacting surface. This type of constraint allows two surfaces to be fused together even when the mesh nodes do not coincide. A master-slave technique was used to keep the two surfaces compatible. The dam wall was chosen as the master surface as it is the primary displacing structure, and the fluid surface being the slave trailing surface (Please refer to Appendix A for theory on Surface based Contact tie technique).

The fluid medium could not be modelled to infinity in the upstream direction, therefore a non-reflective planar Acoustic Impedance boundary was applied on the upstream end surface. It is designed to damp all acoustic hydrodynamic degrees of freedom heading upstream, such that no interferences are inflicted on the solution. The boundary conditions, constraints and interactive surfaces applied to the model are shown in Figure 3.8.

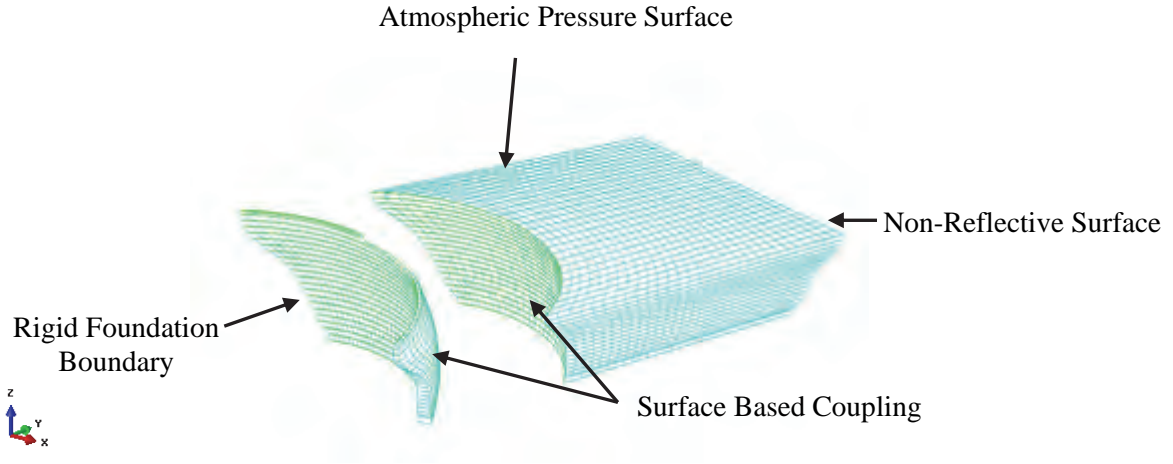


Figure 3.8: Boundary conditions, constraints and interactions applied to the FSI model

3.4 Westergaard Method

The Westergaard method as summarised in section 2.2 requires the added masses to be applied on the upstream side of the dam wall, with a varying parabolic distribution increasing with water depth. Equation 2.7 forms the basis for estimating the added mass at a given node on the up-stream face of the dam. Considering Roode Elsberg Dam, in plan, the dam is made of varying arched circles where the extrados and intrados centres lie along one reference plane (Y-Z plane). Along the elevated long section the dam is parabolic in nature, and is centred at a height of 15.24 m above ground level. In order to find the normal direction cosines of the dam a curvilinear surface created by the intersection of these two geometric shapes had to be considered.

3.4.1 Added mass

The first step was to define the shapes parametrical in polar co-ordinates using algebraic functions. These parametric equations define any point on the upstream surface of the dam. Provided below are equation 3.2 and 3.3 the parametric equations for the circular arches and the parabolic profiles respectively.

$$P_1(\theta_R) = r \cos \theta_R \hat{\mathbf{i}} + (b + r \sin \theta_R) \hat{\mathbf{j}} + h \hat{\mathbf{k}} \quad (3.2)$$

Where

r = Radius of the circle of interest

θ_R = Angle measured from positive X-Axis

h = Height above ground level of considered circular arch

$$P_2(\theta_p) = h \hat{i} + (P \operatorname{Cosec}^2(\frac{\theta_p}{2}) - 1) \hat{j} + (2P \cot(\frac{\theta_p}{2}) + 15.24) \hat{k} \quad (3.3)$$

Where

P = Distance from vertex of parabola to focus and directrix

θ_p = Angle measured from the positive Y-Axis

h = Vertical plane in the X-Axis

In order to determine the normal directional cosine of the arched surface, two vectors lying on the surface had to be determined. Initially, the general tangential vector for each curve had to be determined and the cross product applied to obtain the normal direction cosine for any point on this surface. The general tangential vectors for all points on the respective curves are derived below as equation 3.4 and 3.5:

$$\frac{\partial P(\theta_R)}{\partial \theta_R} = \lambda_1 = r [-\sin \theta_R, \cos \theta_R, 0] \quad (3.4)$$

$$\frac{\partial P_2(\theta_p)}{\partial \theta_p} = \lambda_2 = P [0, \operatorname{Cosec}^2(\frac{\theta_p}{2}) \cdot \cot(\frac{\theta_p}{2}), \operatorname{Cosec}^2(\frac{\theta_p}{2})] \quad (3.5)$$

The unit normal vector at any arbitrary point could be found by applying the cross product to the above vectors λ_1 (vector tangent to r-curve) and λ_2 (vector tangent to p-curve) and normalising the vector by dividing by its length as described below:

$$\vec{n} = \frac{\lambda_1 \times \lambda_2}{|\lambda_1 \times \lambda_2|}$$

The normal to any point on the surface was determined as equation 3.6:

$$\vec{n} = \frac{1}{\sqrt{1 + \sin^2(\theta_R) \cot^2\left(\frac{\theta_P}{2}\right)}} [\cos \theta_R, \sin \theta_R, -\sin \theta_R \cdot \cot\left(\frac{\theta_P}{2}\right)] \quad (3.6)$$

This above equation was substituted into equation 3.). Where M_{Ai} is the added mass matrix derived by Kuo (1982) and is associated with node i .

$$M_{Ai} = \alpha_i A_i \vec{n}_i^T \vec{n}_i \quad (3.7)$$

$$M_{Ai} = \frac{\alpha_i A_i}{1 + \sin^2(\theta_R) \cot^2\left(\frac{\theta_P}{2}\right)} \begin{bmatrix} \cos^2 \theta_R & \cos \theta_R \sin \theta_R & -\sin \theta_R \cos \theta_R \cot\left(\frac{\theta_P}{2}\right) \\ \cos \theta_R \sin \theta_R & \sin^2 \theta_R & -\sin^2 \theta_R \cot\left(\frac{\theta_P}{2}\right) \\ -\sin \theta_R \cos \theta_R \cot\left(\frac{\theta_P}{2}\right) & -\sin^2 \theta_R \cot\left(\frac{\theta_P}{2}\right) & \sin^2 \theta_R \cot^2\left(\frac{\theta_P}{2}\right) \end{bmatrix}$$

It should be noted that the added mass components of the 3x3 matrix were coupled with respect to the nodal degrees of freedom but uncoupled with respect to the individual nodes. The consistent mass matrix (non-diagonal) can be inputted into Abaqus using the User Subroutine feature. The above implementation could easily slow down the computational time of the model. An alternative to this was to use the mass lumping technique which only requires the diagonal mass components of the mass matrix, but are scaled by a factor to preserve the added mass at every node. This would make the added masses independent with respect to the degrees of freedom, giving a better physical representation of the mass and improves the computational time for modelling.

The added mass matrices were lumped using the Hinton, Rock and Zienkiewicz (HRZ) lumping technique. The lumping method is only known to preserve the mass but not the moment of inertia. The method was employed by computing the diagonal entries of the mass matrix where the values were scaled by a factor which is a ratio of the total mass at the node and the trace of the matrix (sum of the diagonals). Provided below is the scaling factor from the method (equation 3.8) and the added mass matrix (equation 3.9) which was employed after mass lumping was conducted using the HRZ method.

$$\beta = \frac{Tot(\sum m_{ab})}{(m_{11} + m_{22} + m_{33})} \quad (3.8)$$

$$M_{Ai} = \frac{\alpha\beta A_i}{1 + \sin^2(\theta_R)\cot^2(\frac{\theta_P}{2})} \begin{bmatrix} \cos^2\theta_R & 0 & 0 \\ 0 & \sin^2\theta_R & 0 \\ 0 & 0 & \sin^2\theta_R\cot^2(\frac{\theta_P}{2}) \end{bmatrix} \quad (3.9)$$

3.4.2 Partitioning of the Dam Wall

The Westergaard method as detailed in section 2.3.1 requires the added masses to be applied on the upstream side of the dam wall, with a varying parabolic distribution increasing with water depth. The dam wall part was partitioned to allow application of the added masses at specific nodal position as shown in figure 3.9 below. The dam wall was partitioned horizontally and vertically on the reference planes provided in the design drawings, this was done as the Westergaard masses varied with radial position and height. Further vertical partitioning was required on the abutment sides, as the water depth changes quite significantly as you move towards the outmost edges of the abutment supports. In total 25 vertical and 22 horizontal partitions were created.

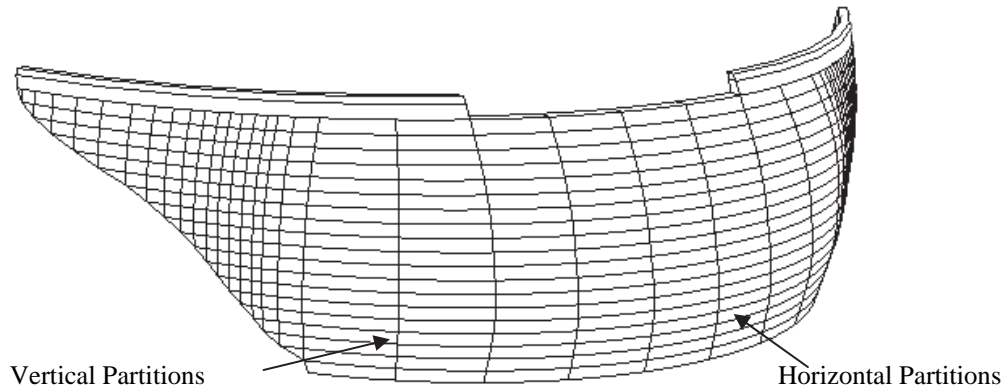


Figure 3.9: Dam wall partitioned to allow for application of the Westergaard added masses.

3.4.3 Application of Inertial Mass

In applying the Westergaard formulation the recommended method is to apply the mass as nodal inertial mass on the wetted upstream surface. Each node must be assigned a tributary area, where the hydrodynamic pressures are assumed to be constant over the tributary area

and have the same magnitude of ‘added mass’ as that of the associated node. The allocation of tributary area to a typical node was dependent on the location and positioning of the node. The nodes were grouped into the following classes: internal, abutment edge, top and bottom edge nodes. The internal nodes were assigned a quarter of each of the surrounding surface partitions (Figure 3.10). The abutment edge nodes were allocated 1/3 of the above and below surface areas and a quarter of the internal partition. Finally, the exterior top and bottom edge nodes were assigned a quarter of the adjacent partitioned areas.

The added masses were assigned in Abaqus using the inertia mass engineering feature. The toolkit allowed point masses (m_{11}, m_{22}, m_{33}) associated with the three translational degrees of freedom (u_1, u_2, u_3), to be applied on element nodes located on the upstream surface.

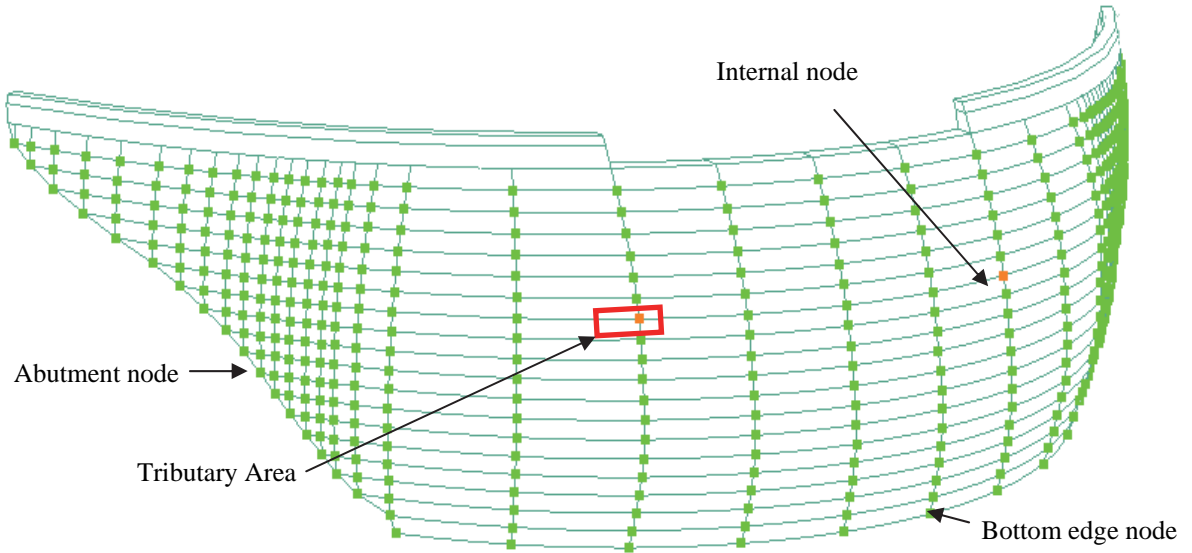


Figure 3.10: Element nodes used to apply the added mass as inertial nodal mass.

3.5 Parametric Study of Reservoir Orientation and Geometry

A parametric study was conducted to investigate the effect of the reservoir orientation and geometry on the dynamic characteristics. Work conducted by Kuo (1982) showed that under seismic loading divergence of the reservoir affects the hydrodynamic pressures exerted on the structure near the abutments and crown position. This parametric study would investigate if a similar phenomenon would be experienced in the ambient condition, and whether it would have an influence on the dynamic properties. It also looked at the effect on the hydrodynamic pressures from an asymmetrical orientated reservoir. The latter was

considered as a case study and would be conducted on the Roode Elsberg which has an asymmetrically orientated reservoir.

The parametric study was investigated using the FSI model created in the comparison study. The reservoir geometry was considered by analysing the effect of a diverging reservoir on the dynamic characteristics. The fluid medium was opened from the prismatic scenario in incremental angles of 10° up until a diverging angle of 40° (Figure 3.11 below). The reservoir orientation was investigated by incrementally skewing the reservoir geometry by 10° up until an angle of 40° (see Figure 3.11 below).

Diverging and Asymmetric Reservoir

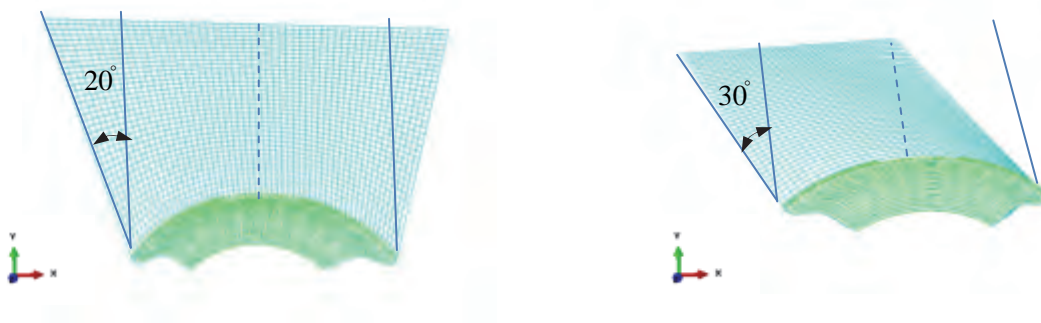


Figure 3.11: Diverging and asymmetric cases considered in the parametric study.

3.6 Results and Discussion of hydrodynamic analysis

3.6.1 Natural frequencies and mode shapes

Table 3.4 shows the first six natural frequencies obtained from ambient vibration tests (AVT), fluid structure interaction, and the Westergaard method. The ambient vibration tests were carried out on 10 September 2013 with the dam 100% full. A comparison between the natural frequencies, shows that the Westergaard formulation produces natural frequencies that are approximately 20% less than measured natural frequencies while the FSI model yields natural frequencies within about 1.5% of the measured frequencies. The fluid

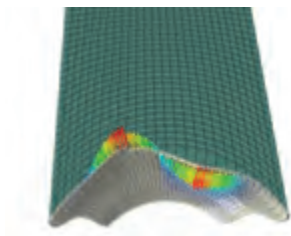
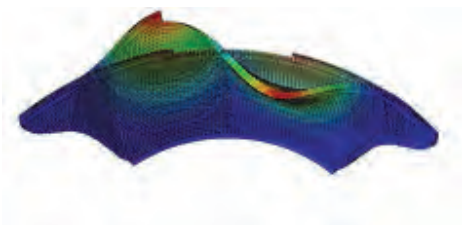
structure interaction approach clearly agrees closely with measured data. This confirms earlier results that the Westergaard overestimates added mass and thus not appropriate for estimating natural frequencies under operating conditions.

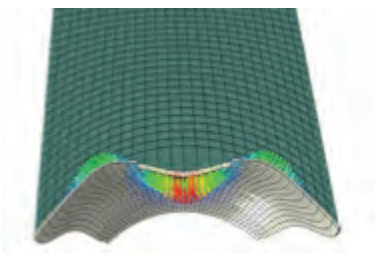
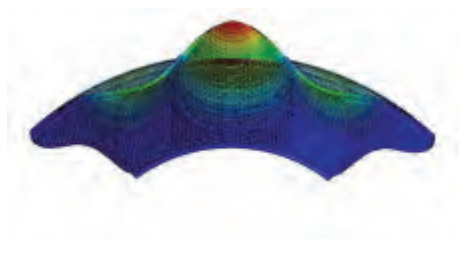
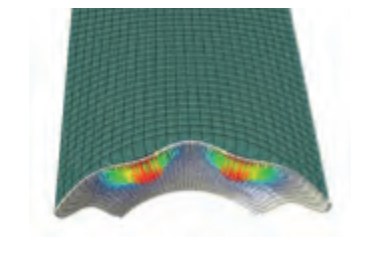
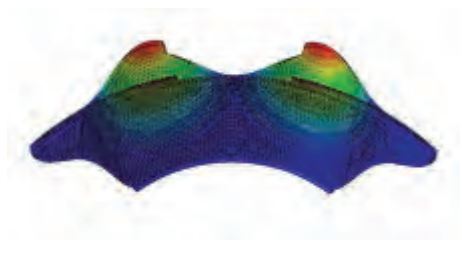
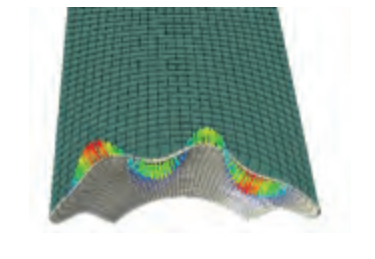
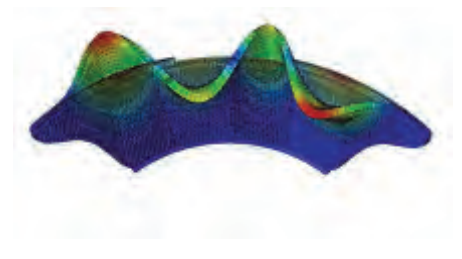
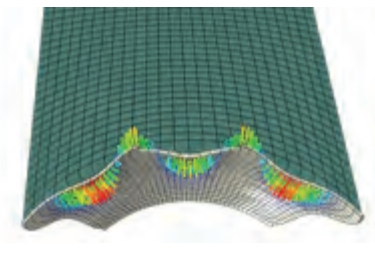
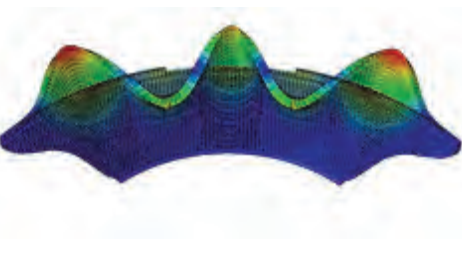
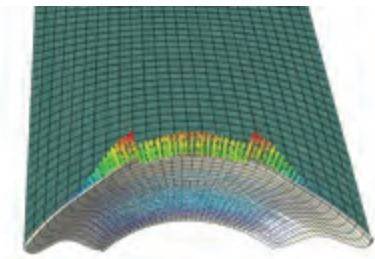
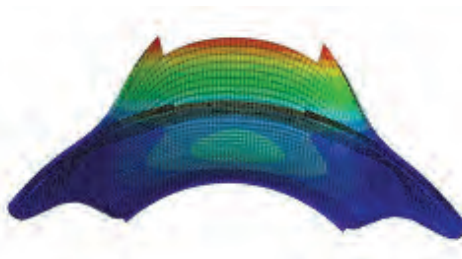
Table 3.5 shows mode shapes obtained from the fluid structure interaction approach and the Westergaard Method confirming the pairing of natural frequencies in Table 3.4.

Table 3.4: Comparison of natural frequencies (Hz) obtained from AVT test in Sep-2013 with the FSI model and Westergaard method.

Modes	AVT 10-09- 2013	FSI Model	Westergaard	FSI % Error	Westergaard % Error
1	3.05	2.96	2.34	2.81	23.28
2	3.23	3.23	2.50	0.05	22.52
3	4.43	4.49	3.60	1.44	18.71
4	5.62	5.54	4.62	1.41	17.71
5	6.50	6.67	5.56	2.61	14.40
6	7.23	7.20	5.77	0.43	20.18

Table 3.5: Comparison of natural frequencies (Hz) obtained from AVT test in Sep-2013 with the FSI model and Westergaard method.

Mode	FSI	Westergaard
1	 <p>2.96 Hz</p>	 <p>2.34 Hz</p>

2	 <p>3.23 Hz</p>	 <p>2.50 Hz</p>
3	 <p>4.49 Hz</p>	 <p>3.60 Hz</p>
4	 <p>5.54 Hz</p>	 <p>4.62 Hz</p>
5	 <p>6.67 Hz</p>	 <p>5.56 Hz</p>
6	 <p>7.20 Hz</p>	 <p>5.77 Hz</p>

3.6.2 Effect of reservoir geometry on natural frequencies

The study was conducted to assess whether the modal parameters and hydrodynamic pressures acting on the arch dam wall would be influenced by the geometry and orientation of the reservoir under ambient conditions. A parametric study conducted by Kuo (1982) showed that under seismic loading the hydrodynamic pressures decrease as the reservoir geometry diverged. This would have to be clarified before a case study would be conducted on the Roode Elsberg dam, where the reservoir is diverging and asymmetric.

Table 3.6 shows the natural frequencies obtained in the diverging reservoir parametric study. The results obtained show that the natural frequencies do not change significantly as the impounded water body geometry is opened in incremental angles of 10° . The general trend is that the natural frequencies increase marginally as the reservoir geometry diverges.

Table 3.6: Natural Frequency (Hz) from diverging parametric study

Mode	Ref	10 Deg Div	20 Deg Div	30Deg Div	40 Deg Div
1	2.96	2.96	2.97	2.97	2.97
2	3.23	3.23	3.23	3.23	3.23
3	4.49	4.49	4.49	4.49	4.50
4	5.54	5.54	5.55	5.55	5.55
5	6.67	6.68	6.68	6.69	6.69
6	7.20	7.21	7.21	7.21	7.22

Similar results are observed when orientating the reservoir asymmetrically behind the dam. The first 3 angles produced insignificant change in the properties (Table 3.6). The reservoir skewed at an orientation of 40° produced technical difficulties in the modelling phase as regions of the foundation canyons would intersect with the geometry of the dam, this being unacceptable. It may be concluded that this is an excessive skew, which is physically not practical, as portions of the fluid at that specific orientation could not be modelled. While the magnitude of change in the natural frequencies is low, there general trend is a slight decrease in natural frequency due to asymmetric reservoir.

Table 3.7: Natural Frequency (Hz) from asymmetric parametric study

Mode	Ref	10 Deg Asym	20 Deg Asym	30 Deg Asym
1	2.96	2.96	2.95	2.94
2	3.23	3.23	3.22	3.22
3	4.49	4.49	4.48	4.47
4	5.54	5.54	5.52	5.52
5	6.67	6.67	6.63	6.63
6	7.20	7.20	6.96	6.96

The results obtained from the parametric study show that the orientation and geometry of the reservoir have an insignificant effect on the natural frequencies. This is supported by the first 6 natural frequencies of the diverging and asymmetric study (Tables 3.6 & 3.7). The hydrodynamic pressure distribution acting on the dam wall were analysed to explain the observed behaviour of the dynamic properties. The distribution of pressure was extracted at the crown, quarter arc and abutment edges on the upstream side of the wall. The first 3 modes of the reference, diverging and asymmetric models were analysed.

3.6.3 FSI Hydrodynamic Pressure Distribution

Figures 3.12, 3.13 & 3.14 show the pressure distribution as a function of depth plotted for modes 1-3 for the case of a symmetrical reservoir. In all cases the dynamic pressures acting at the quarter arc position have a complex distribution which is not a parabolic shape as that proposed by Westergaard (1933) for dam walls under seismic loading. The maximum pressure occurs at approximately 18 m below the water surface level for modes 1&2.

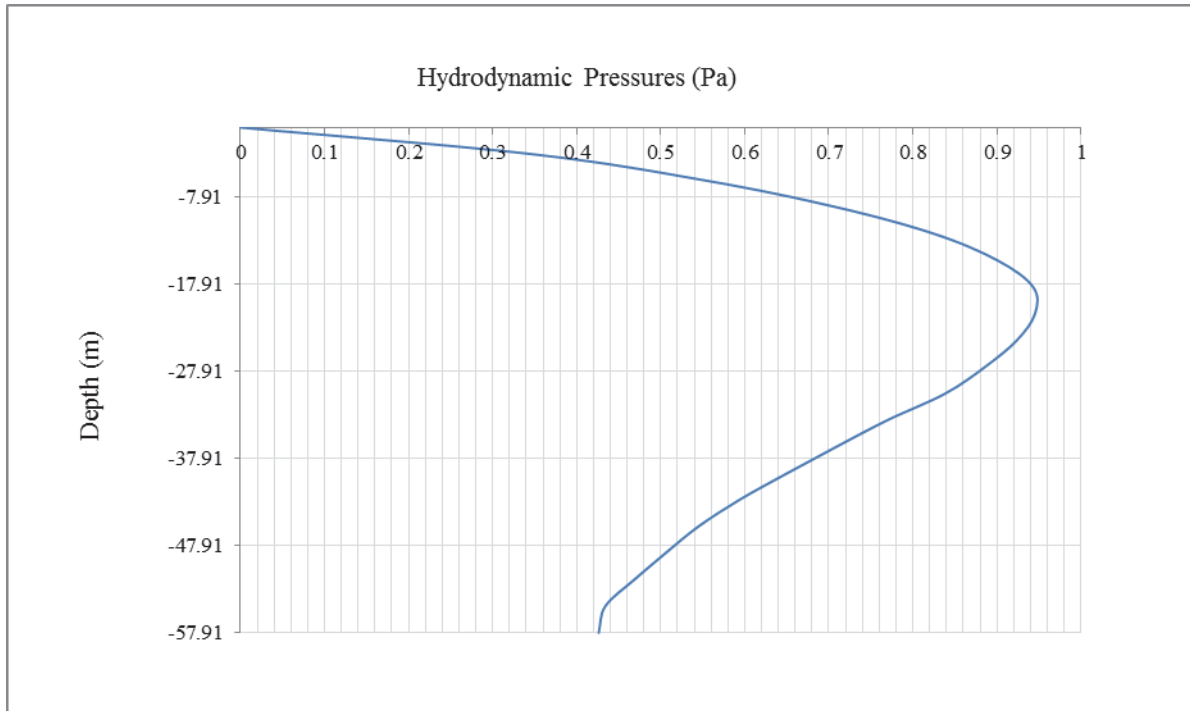


Figure 3.12: Pressure distribution at quarter arc location for Mode 1

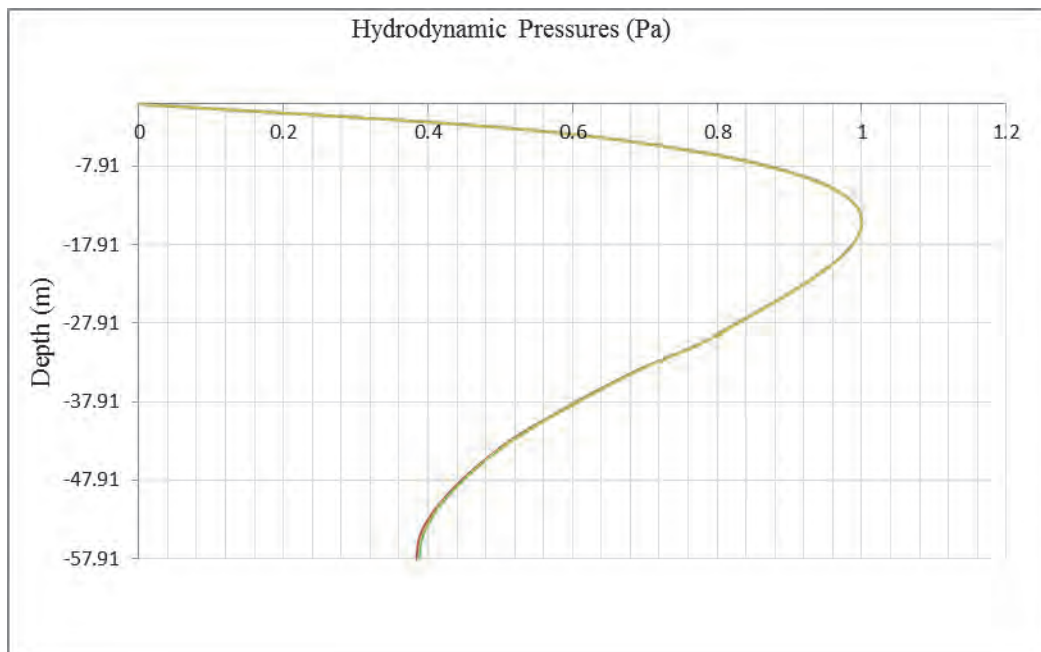


Figure 3.13: Pressure distribution at crown level for mode 2.

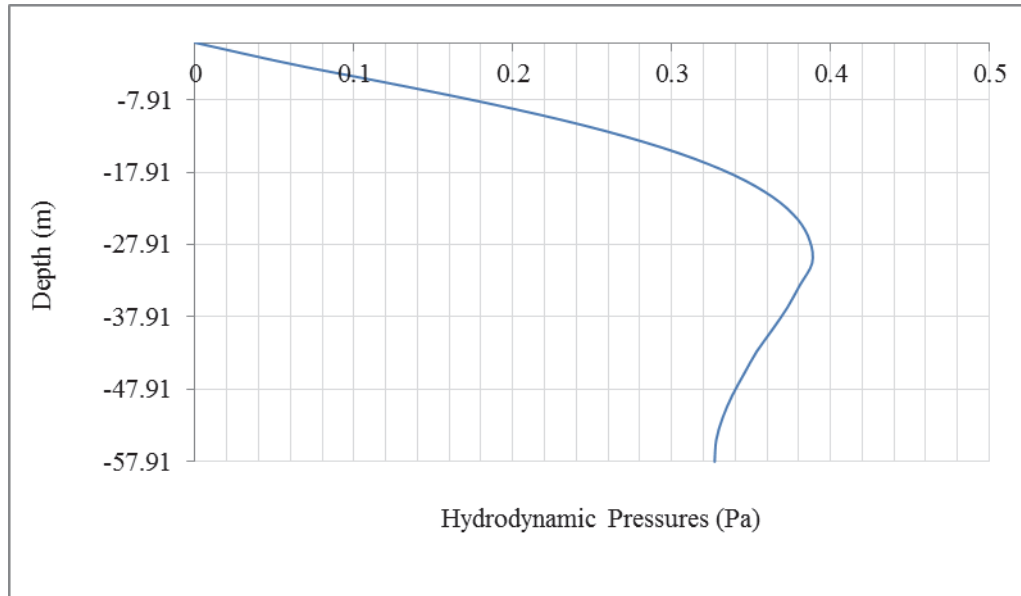


Figure 3.14: Pressure distribution at crown position for mode 3

The results obtained from this parametric study clarify that the hydrodynamic behaviour experienced in seismic conditions differs from that in the ambient state. Firstly, the distribution of pressure is not of a parabolic nature that was proposed by Westergaard (1933) and described by Kuo (1982). The distribution of pressure in the ambient state is dependent on the location of the arch and the behaviour of the mode. The diverging and asymmetry of the reservoir have an insignificant effect on the natural frequencies of the dam with a maximum increase of 0.58% and decrease of 2.48% respectively.

3.7 Summary

In summary, this chapter contains the results and discussion that carry out the objectives of this work. Initially we assessed the behaviour of the acoustic finite elements as a suitable option of representing the impounded water body. Thereafter the objectives of this work were carried out, these included; (i) Comparison of the hydrodynamic methods, (ii) evaluating the effect of a reservoir orientation and geometry on the dynamic characteristics of an arch dam, (iii) Development of the dynamic finite element models of the Roode Elsberg arch dam (iv) Validation of the Roode Elsberg finite element models using as built operational modal parameters obtained from ambient vibration testing.

4 CONTINUOUS MONITORING OF ROODE ELSBERG DAM

4.1 Introduction

A suite of static monitoring instrumentation has been in operation since 1984. They include, clinometers and pendulum clinometer, geodetic survey targets, crack gauges as well as Trivecs. The latest additions in 2010 and 2013 respectively are; a continuously monitored GPS system at four survey beacons and an ambient vibration measurement (AVM) system. In addition, there is a weather station to monitor the ambient conditions at the dam and also a system to measure water temperatures.

4.2 Description of the dynamic monitoring system

The ambient vibration monitoring system consists of three force balanced of tri-axial accelerometers (Figure 4.1) with a dynamic range of more than 125 dB at ± 2 g full scale within a frequency range of 0.1 Hz to 50 Hz. The accelerometers are connected to a 24bit digitizer which communicates with the industrial computer. The data acquisition system (industrial computer and the digitizer) is placed on the dam wall inside the upper gallery of the dam to avoid any environmental effects (Figure 4.1). The data is sampled at 50 Hz and stored at hourly intervals.



Figure 4.1: Accelerometers on the dam crest and data acquisition system in the upper dam gallery

4.3 Description of Global Navigation Satellite System

Displacements of Roode Elsberg have been monitored by Department of Water Affairs and Sanitation (DWA) using geodetic survey methods twice a year since 1984. In 2010 the Department implemented an automatic deformation monitoring system on the dam using Global Navigation Satellite Systems (GNSS) as shown in Figure 4.2. The system comprises of the following:

- i. Four GNSS receivers, each powered by solar energy and two 12 V batteries, two secondary sensors on the crest of the dam structure, one on each side of the spillway and two base station sensors up and downstream of the dam wall;
- ii. Poynting Wi-Fi network streaming all the receiver data to a server in a central control room; and

The two secondary GNSS sensors on the crest of the dam wall (P203 on left flank and P206 on right flank) are used to calculate real-time kinematic positions of the points and to detect any sudden movement at the crest of the dam, as well as the base points. The two base GNSS sensors up and downstream of the dam wall are used as fixed stations. All the satellite data is accessible to DWS staff via a web interface.



Figure 4.2: GPS network on Roode Elsberg dam

Two base stations (Figure 4.2) were set up on the existing Geodetic Deformation network stations of the dam, and run continuously. These base stations are used as reference stations for the relative positioning in the post-processing mode. The base stations are occupied permanently in order to achieve high accuracy in the estimation baseline lengths between base stations. Figure 4.3 shows base station P01.



Figure 4.3: Base station P01 on Roode Elsberg dam

4.4 Measurement of environmental and operation factors

Water levels on Roode Elsberg dam are measured by simple elevation gauges i.e. level staff gauges (Figure 4.4). The fluctuation levels of the Roode Elsberg reservoir have been monitored on a daily basis since 1974. For this report, only water levels from the 25th November 2013 are considered as this ties with the installation of the dynamic monitoring system. A weather station (Figure 4.5) was installed on 25th November 2013, on the dam crest to measure ambient temperatures and there are thermometers that are embedded into the dam wall to measure reservoir water temperatures at different water levels.



Figure 4.4: Staff gauges for water level measurements



Figure 4.5: Weather station installed on the dam crest near the spillway

4.5 Results and discussions

This report is focussed on the continuous monitoring systems installed on the dam, namely, the GPS system, the AVM system and the temperature monitoring system. At least one year and half of reliable monitoring data is now available from the continuous monitoring system at Roode Elsberg dam. This provides an opportunity to understand the normal condition of the dam structure i.e., how the structure responds to normal variations in environmental and operational conditions. The results are divided into two main sections namely, summary of loading (water level and temperature) observations, summary of response observations and their association with loading.

4.5.1 Reservoir Level

Figure 6.1 shows variation of the reservoir level over the period of interest (November 2013-June 2015). The reservoir level is characterised by a long period of full capacity (June-December 2014). It is also noted that the dam level went below 25 m in 2015 where as it remained above 40 m in 2014.

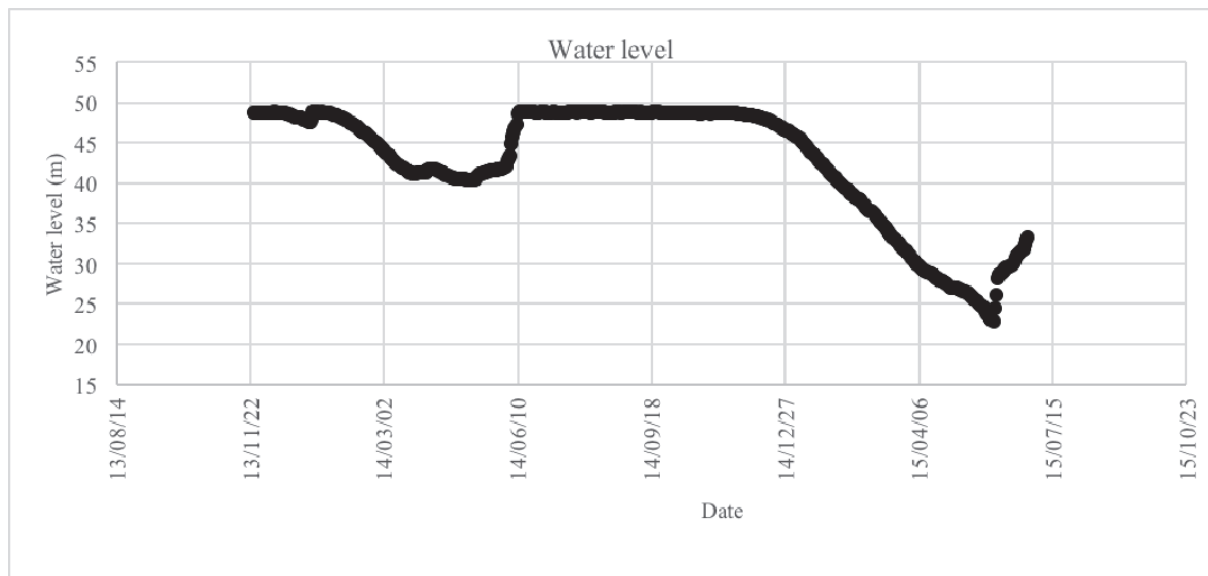


Figure 4.6: Water level

4.5.2 Ambient and reservoir temperatures

Figures 4.3-4.5 show average daily temperatures of the reservoir and the environment. Clearly the deeper temperature sensors show little variability as they are not directly

exposed to the environment. The intermediate locations WT5, WT4, WT3 experience both fully exposed conditions and fully submerged conditions. Based on the observations of variability in the temperature readings, ambient temperature readings will be used for further analysis as they are dependent only one environmental exposure. Figures 4.4-4.5 show temperature data smoothed using a monthly moving average. Note the phase difference between ambient temperature measurements and the reservoir temperature. A precise analysis of the relationship between ambient temperature is not carried out in this report.

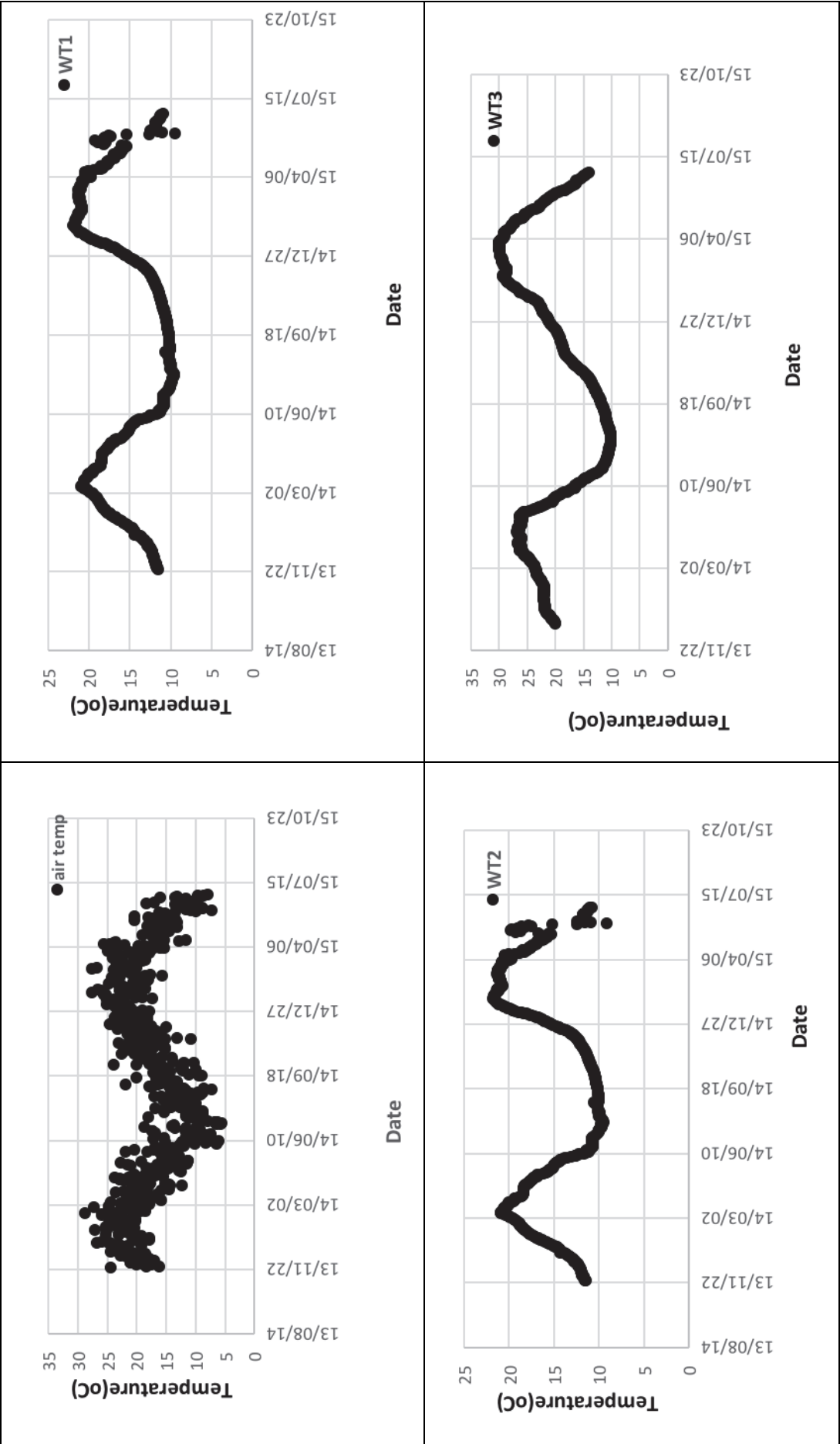


Figure 4.7: Ambient and reservoir temperature variation

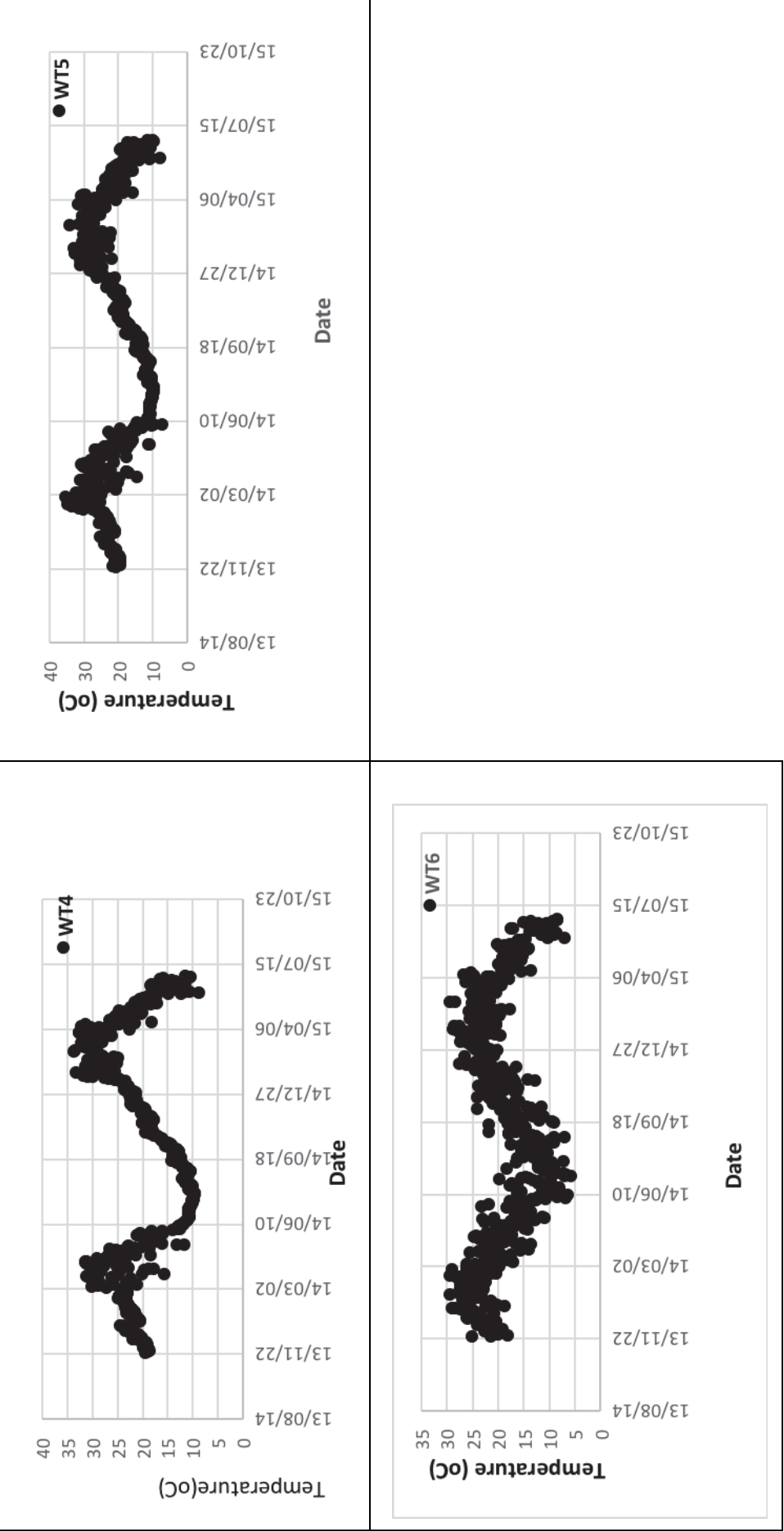


Figure 4.8: Reservoir temperature variation

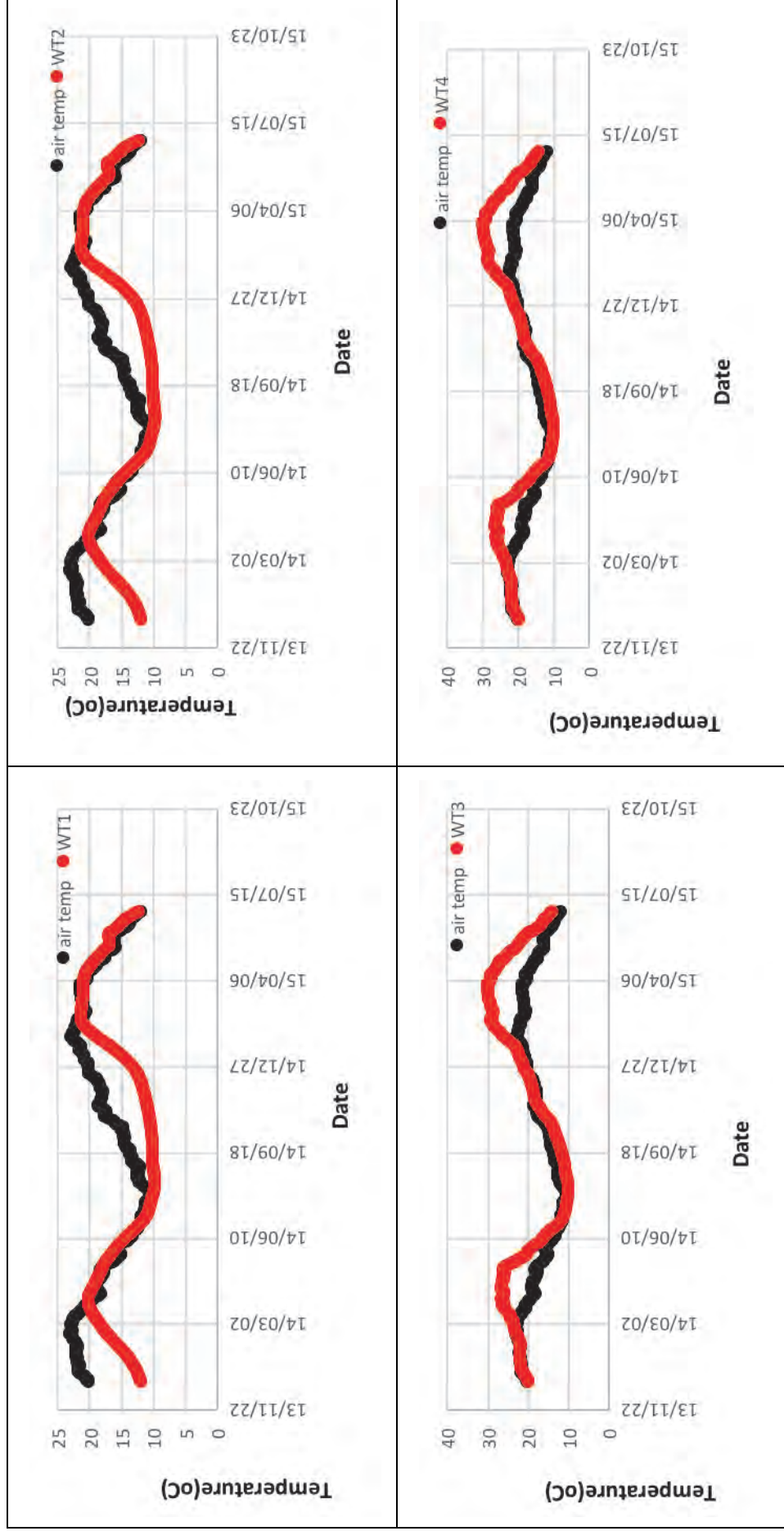


Figure 4.9: Smoothed temperature variation

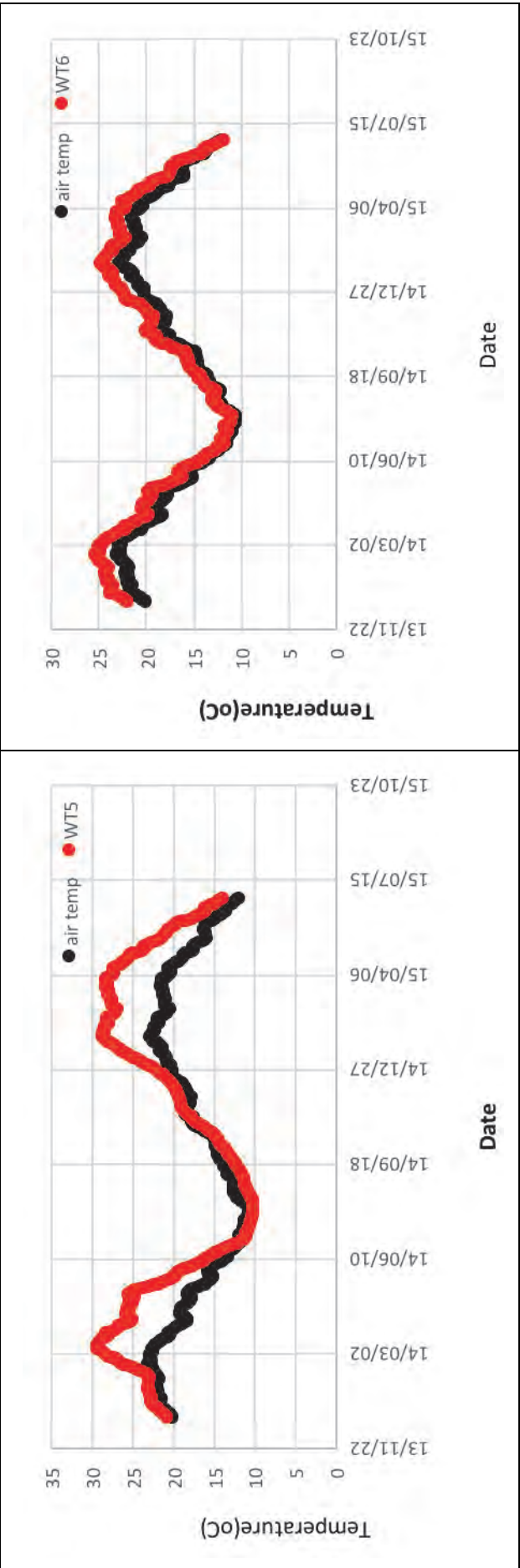


Figure 4.10: Smoothed temperature variation

4.5.3 Dynamic response

The dynamic response (natural frequencies) were extracted from acceleration time series recorded by the dynamic monitoring system. Data driven stochastic subspace identification (SSI-data) method was used to estimate the natural frequencies of the dam. SSI-data method is one of the time based output-only modal analysis methods that utilizes stabilization diagrams to estimate the modal parameters (Zhang et al., 2005). This technique has been shown to perform better than other out-put only techniques such as frequency domain techniques (Bukanya, 2009). Figure (4.11) shows typical singular values of spectral densities of the recorded accelerations. Figure (4.12) shows a typical stabilization diagram used in the estimation of the natural frequencies using the SSI-data method.

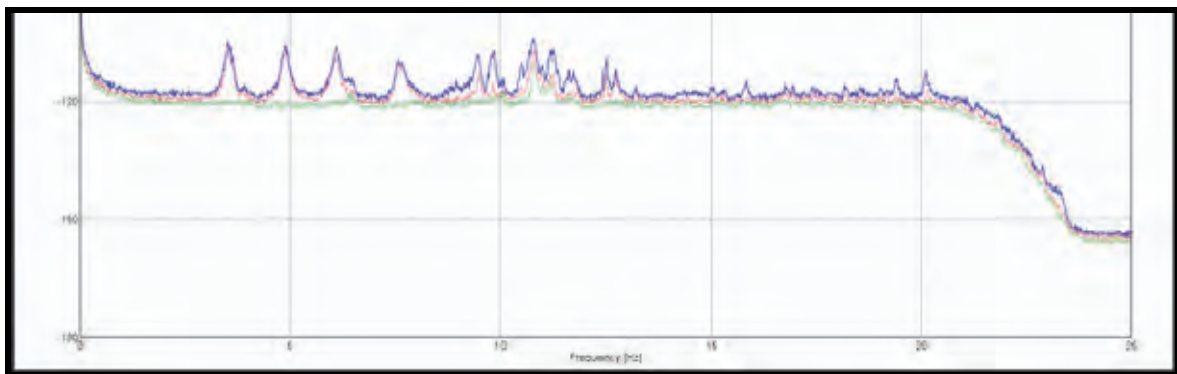


Figure 4.11: Singular values of spectral densities from observed data

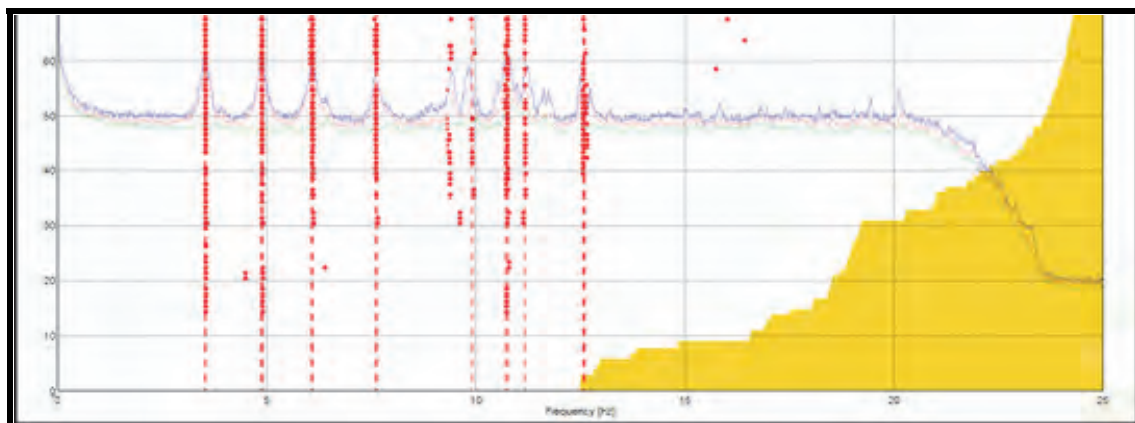


Figure 4.12: Sample Stabilization diagram

The time variation of the first three natural frequencies during the 19 month period is shown in Figures 4.13, 4.14 & 4.15. The first three natural frequencies show strong relationship between dynamic behaviour and the reservoir level (Figure 6.11). The influence of temperature variation on dynamic properties of the dam is not obvious from a comparison

of temperature data to natural frequency data. However, a closer observation of the variation of modes with time in the period, June 2014 to November 2014 shows a slight increase in the natural frequency with the water level almost constant. The average monthly temperature increased during this period and thus, it can be concluded that temperature change lead to change in natural frequency.

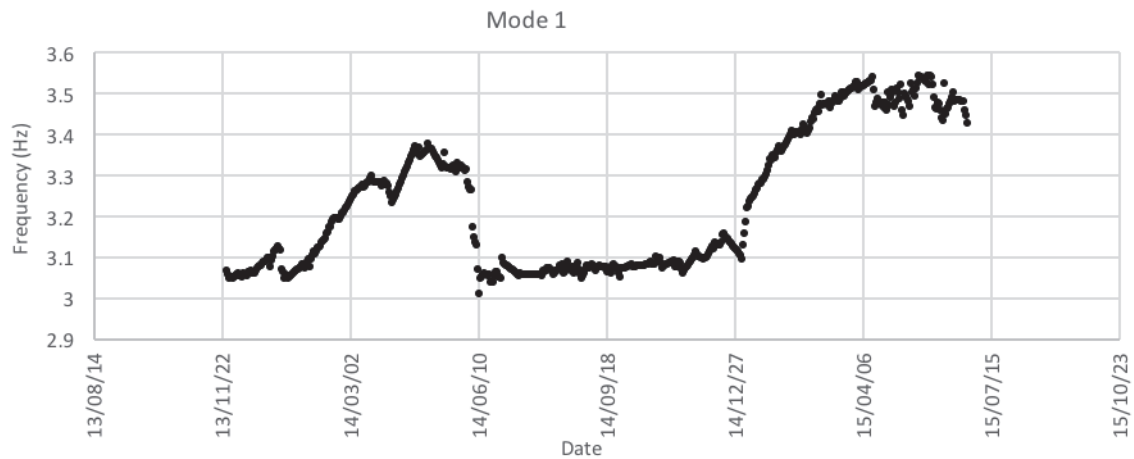


Figure 4.13: Variation of mode 1 with time

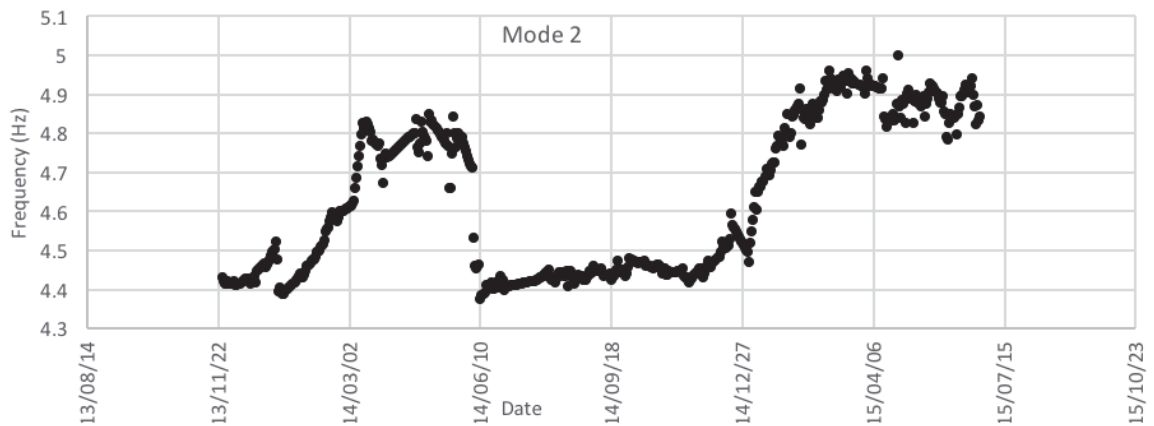


Figure 4.14: Variation of mode 2 with time

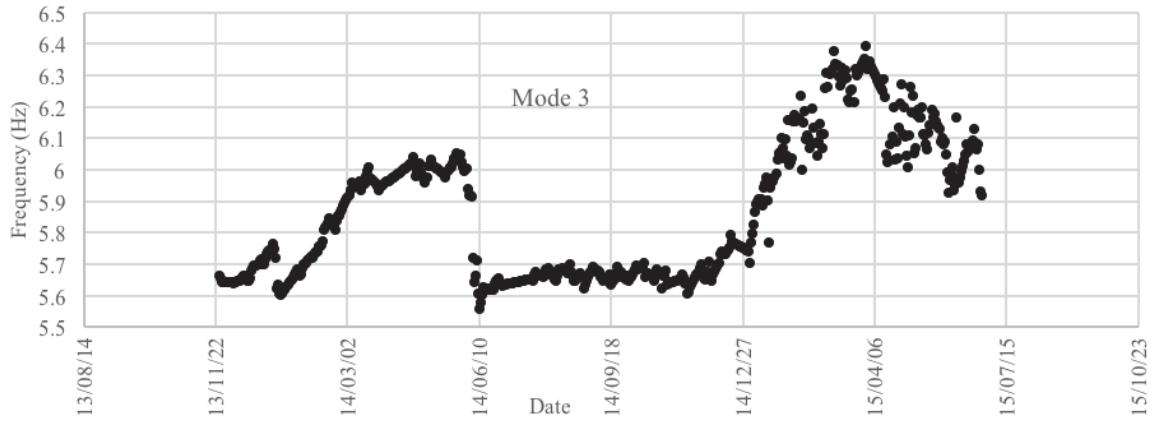


Figure 4.15: Variation of mode 3 with time

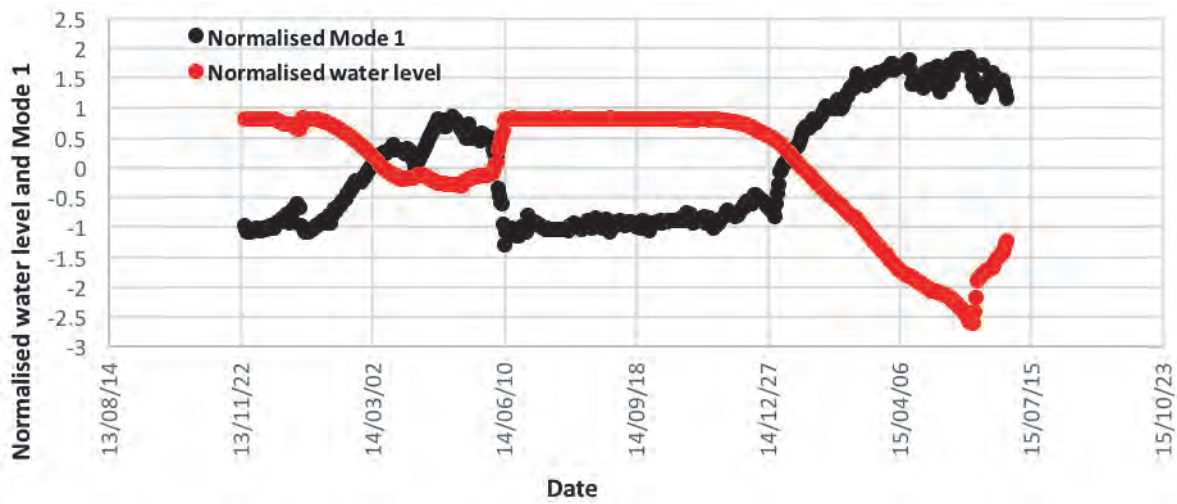


Figure 4.16: Variation of mode 1 and water level with time

4.5.4 Static response

The data available for the present study is for the period January-November 2014. The data is not scaled to absolute displacements and thus presented as normalised values. The data was normalised using the mean and variance. Figures 20-22 show the variation of normalised displacements over a period of 10 months, i.e. from January 2014 to end of November 2014. The data shows a strong dependency of displacements on temperature variations (Figure 4.19) and a weak influence of the reservoir level on dam seasonal displacements (Figure 4.20). Notice however, the influence of the reservoir level on displacements during the rapid increase of reservoir level from approximately 41 m to 48 m

in 10 days of the first week of June 2014. Thereafter, the influence of the water level is not obvious.

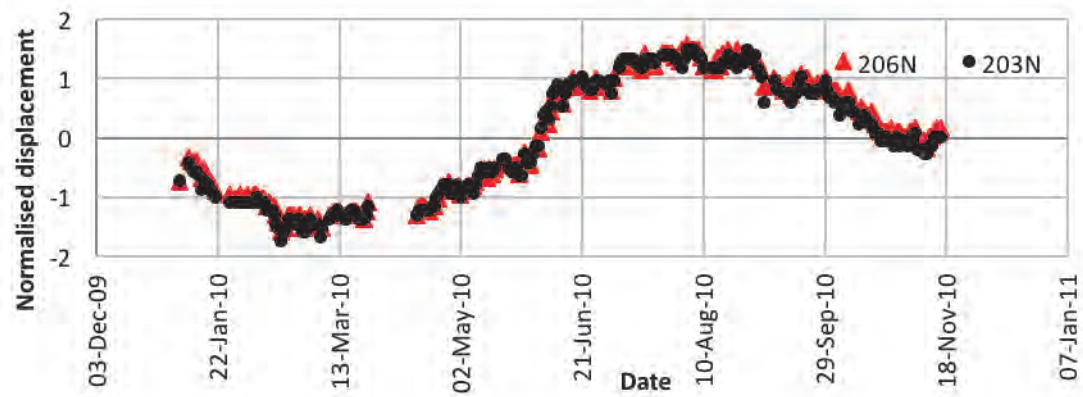


Figure 4.17: Normalised displacements in the radial direction

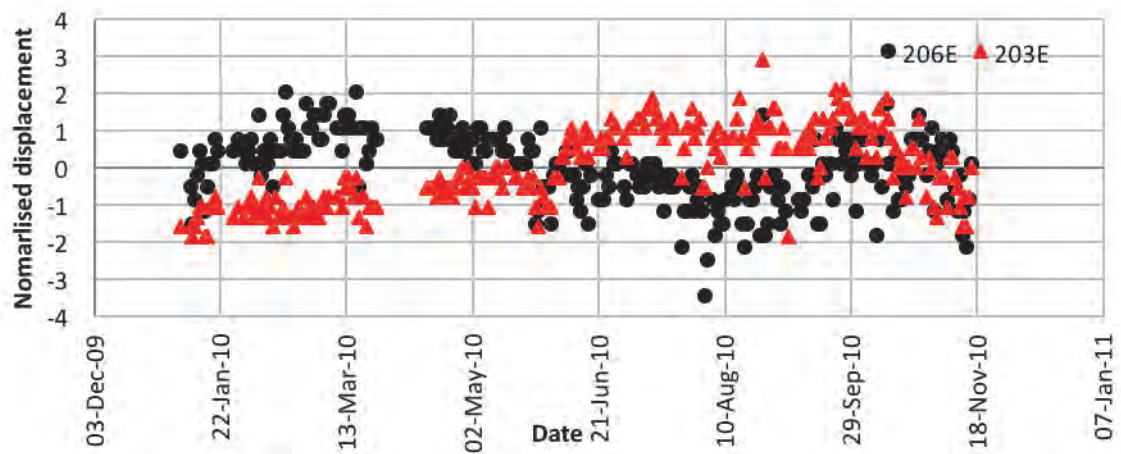


Figure 4.18: Normalised displacements in the tangential direction

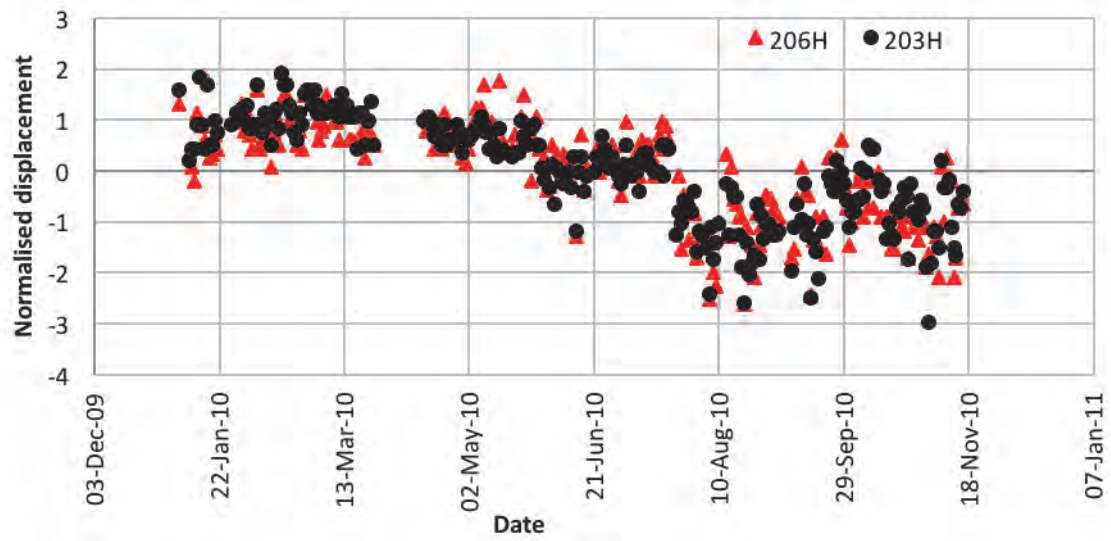


Figure 4.19: Normalised displacements in the vertical direction

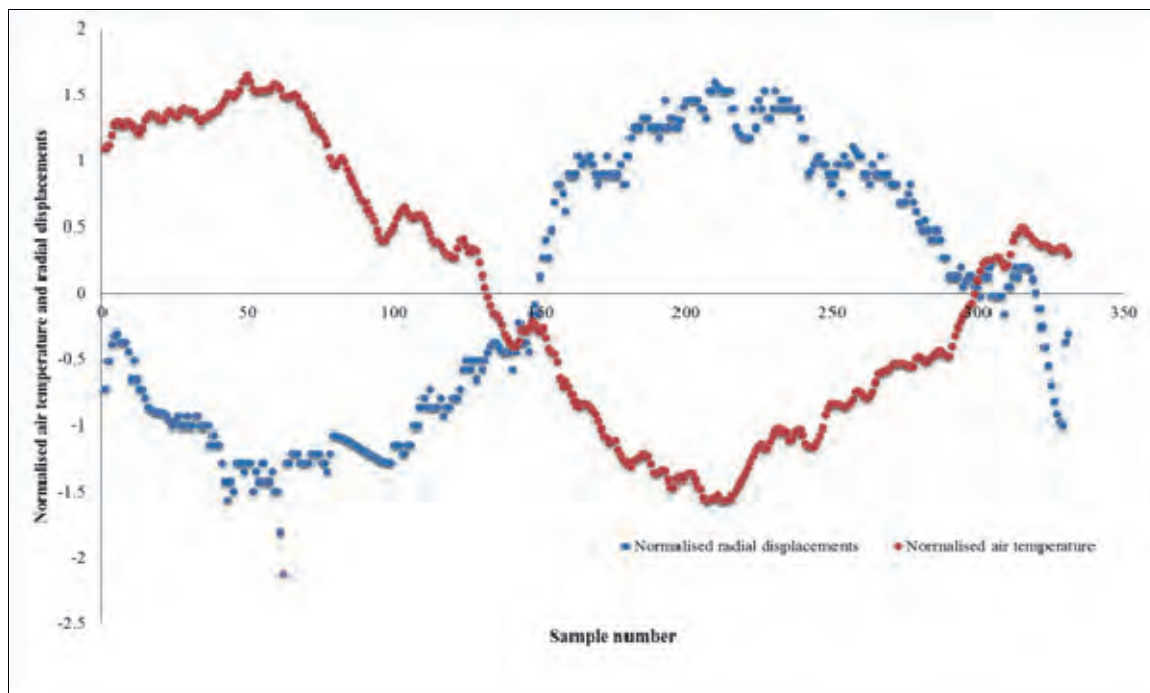


Figure 4.20: Normalised displacements in the radial direction and air temperature

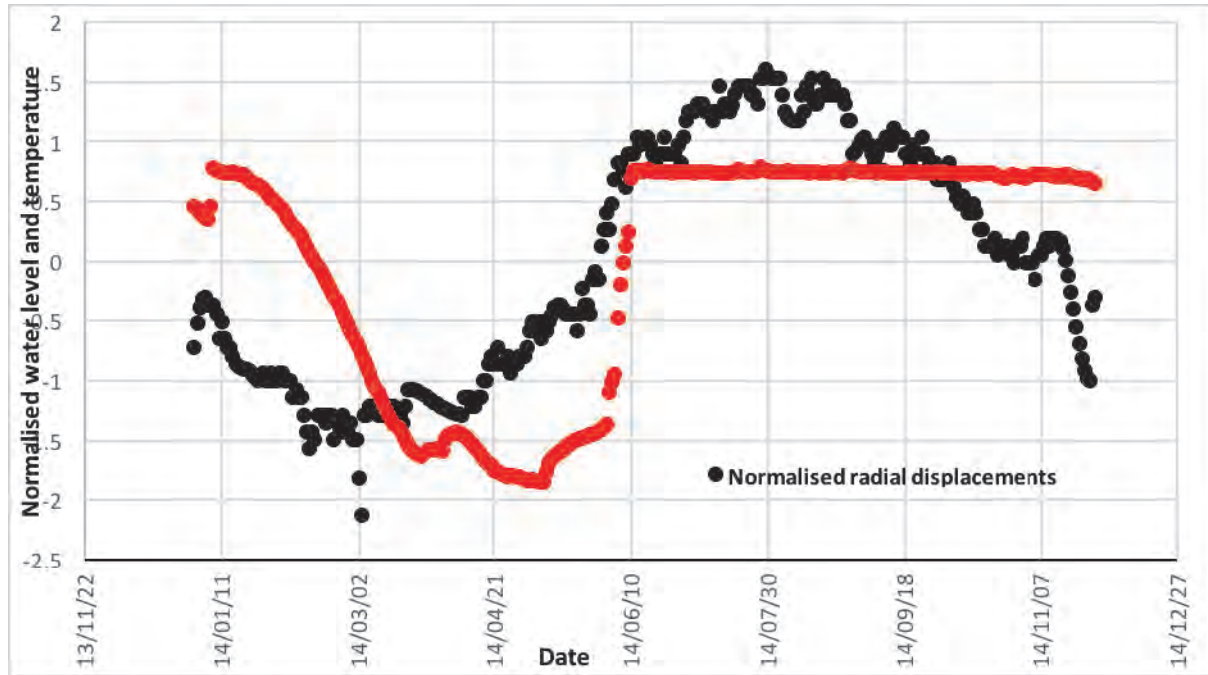


Figure 4.21: Normalised displacements in the radial direction and water level

4.6 Summary of observations

The following key observations are made from the continuous monitoring data;

- The dynamic behaviour of the dam is strongly dependent on the reservoir level. The natural frequencies of the dam decrease with water level. The dam's dynamic behaviour is weakly influenced by temperature variation.
- The seasonal deformation of the dam is strongly dependent on temperature variation. While the seasonal variation of deformations is largely driven by temperature variation, the reservoir level does influence the deformation of the dam especially as the dam fills rapidly.

5 STATISTICAL MODELLING

Continuous monitoring of dams provides information that can be used to; 1) detect the onset of anomalous behaviour, 2) predict future behaviour of the dam based on current and previous observations. Such decisions are best made on the basis of a scientific approach employing robust statistical models in order to minimise false alarms and unreliable predictions. In the case of Roode Elsberg Dam, there is interdependency between measured parameters. The measured parameters can be grouped into two categories namely, the load or input (temperature and reservoir level) and the response or output (displacement and natural frequency). Preliminary analysis described in Chapter 6 of this report shows that natural frequencies are strongly dependent on water level and weakly dependent on temperature. Figure 5.1 is a plot of water level versus natural frequency and there is a clear relationship between the two parameters. On other hand, Figure 5.2 shows the weak relationship between natural frequency and monthly average temperature. Similarly, Figure 5.3 is a plot of displacement versus monthly average temperature and confirms the strong relationship between the two parameters while Figure 7.4 confirms the relationship between displacement and water level. Thus statistical models of both natural frequency and static deformation should be used to track the behaviour of the dam for the purposes of anomaly detection and response forecasting. The most appropriate models would be those that incorporate measured influencing variables for each response. In this case multiple regression models would be plausible. However, transfer function models as well as artificial neural networks could also be investigated in future.

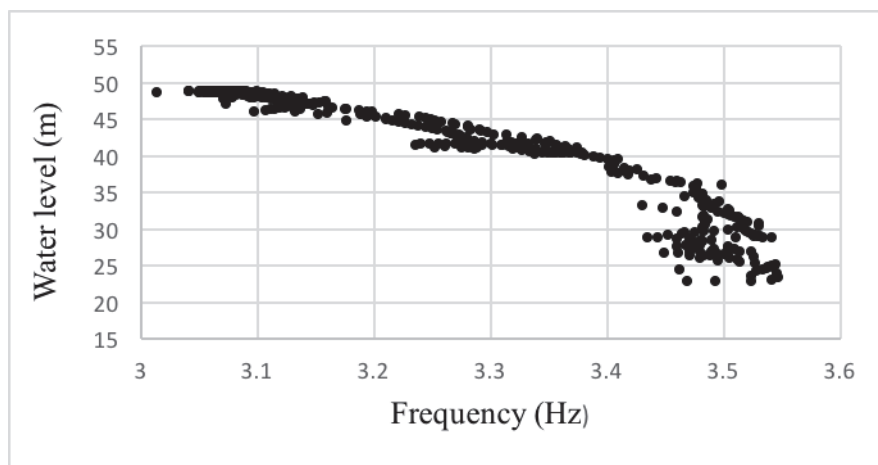


Figure 5.1: Water level versus mode 1

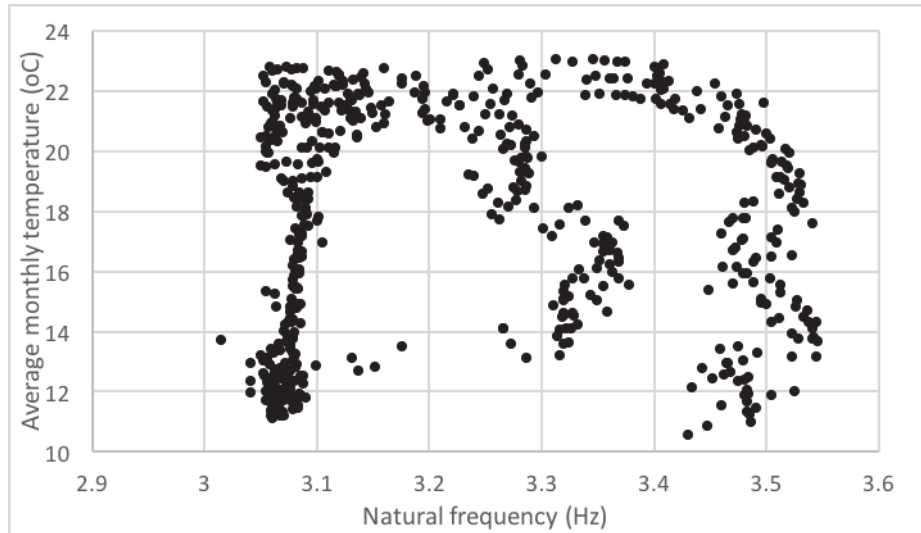


Figure 5.2: Air temperature vs mode 1

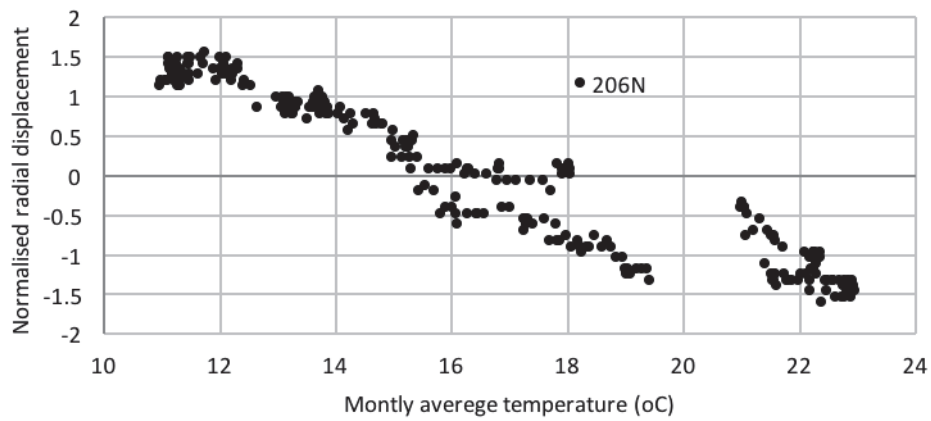


Figure 5.3: Normalised radial displacement versus monthly average air temperature

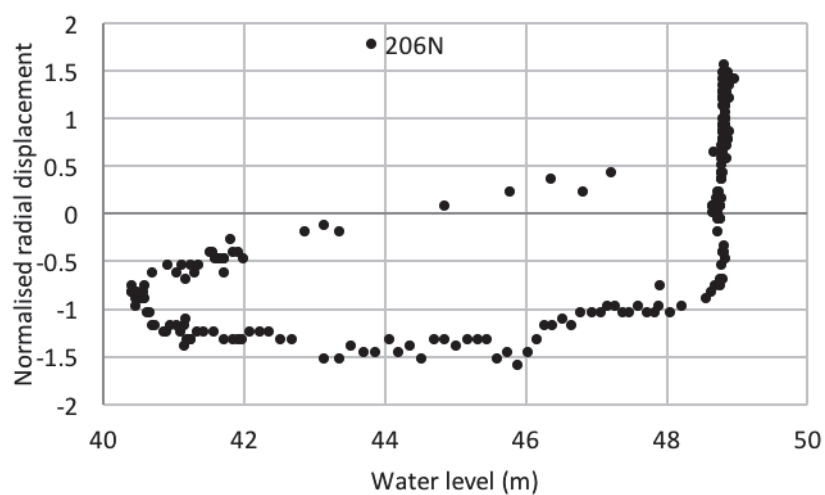


Figure 5.4: Normalised radial displacement versus monthly average air temperature

Based on data exploration carried out in Chapter 6 of this report and following Bonelli and Poyet (2001), natural frequency (ω_t) and deformation (δ_t) consists of reservoir level effect $Y_1(h)$, monthly average temperature effect $Y_2(T)$, a creep and permanent deformation function effect $Y_3(t)$, and an error term $\varepsilon(t)$ as follows;

$$\omega_t = Y_1(h) + Y_2(T) + Y_3(t) + \varepsilon(t) \quad (5.1)$$

$$\delta_t = Y_1(h) + Y_2(T) + Y_3(t) + \varepsilon(t) \quad (5.2)$$

- (1) The effect of the water level can be approximated using a polynomial function which is dependent on a parameter h defined in equation 5.3 Batista et al. (2002)

$$Y_1(h) = \beta_0 + \beta_1 h + \beta_2 h^2 + \beta_3 h^3 + \beta_4 h^4$$

$$h = \frac{H_i - H_{min}}{H_{max} - H_{min}} \quad (5.3)$$

Where $\beta_1, \beta_2, \beta_3, \beta_4$ are the coefficients, H_i is the water level at day i , H_{max} and H_{min} are the maximum and minimum water levels attained during the time of measurement.

- (2) The seasonal temperature effect $Y_2(T)$ is dependent on the monthly moving average temperature and can be approximated using the first terms of the Fourier transform as follows;

$$Y_2(T) = \beta_5 \sin(d) + \beta_6 \cos(d) + \beta_7 \sin^2(d) + \beta_8 \sin(d) \cos(d) \quad (5.4)$$

$$d = \frac{2\pi k}{365}$$

where k is the number of days between the beginning of the year (January 1) until the date of observation and $\beta_5, \beta_6, \beta_7, \beta_8$ are coefficients

- (3) $Y_3(t)$ is the time effect related to concrete creep which can be expressed as:

$$Y_3(t) = \beta_9 \theta + \beta_{10} \ln(\theta + 1) \quad (5.5)$$

where is θ the number of days since the beginning of the analysis but increases by 0.01 each day, β_9, β_{10} are coefficients

The coefficients $\beta_0 \dots \beta_{10}$ of the resulting multi linear regression model can be estimated using the step-wise least squares method. Table 5.1 shows the coefficients obtained for equations 5.1 and 5.2.

Table 5.1: Coefficients of linear regression

	Natural frequency coefficients	Displacement coefficients
β_0	2.52	33.38
β_1	7.17	-178.3
β_2	-16.70	353.4
β_3	15.23	-312.2
β_4	-5.14	104.05
β_5	-0.029	-0.563
β_6	-0.0054	-0.839
β_7	-0.0372	-0.239
β_8	-0.0245	0.219

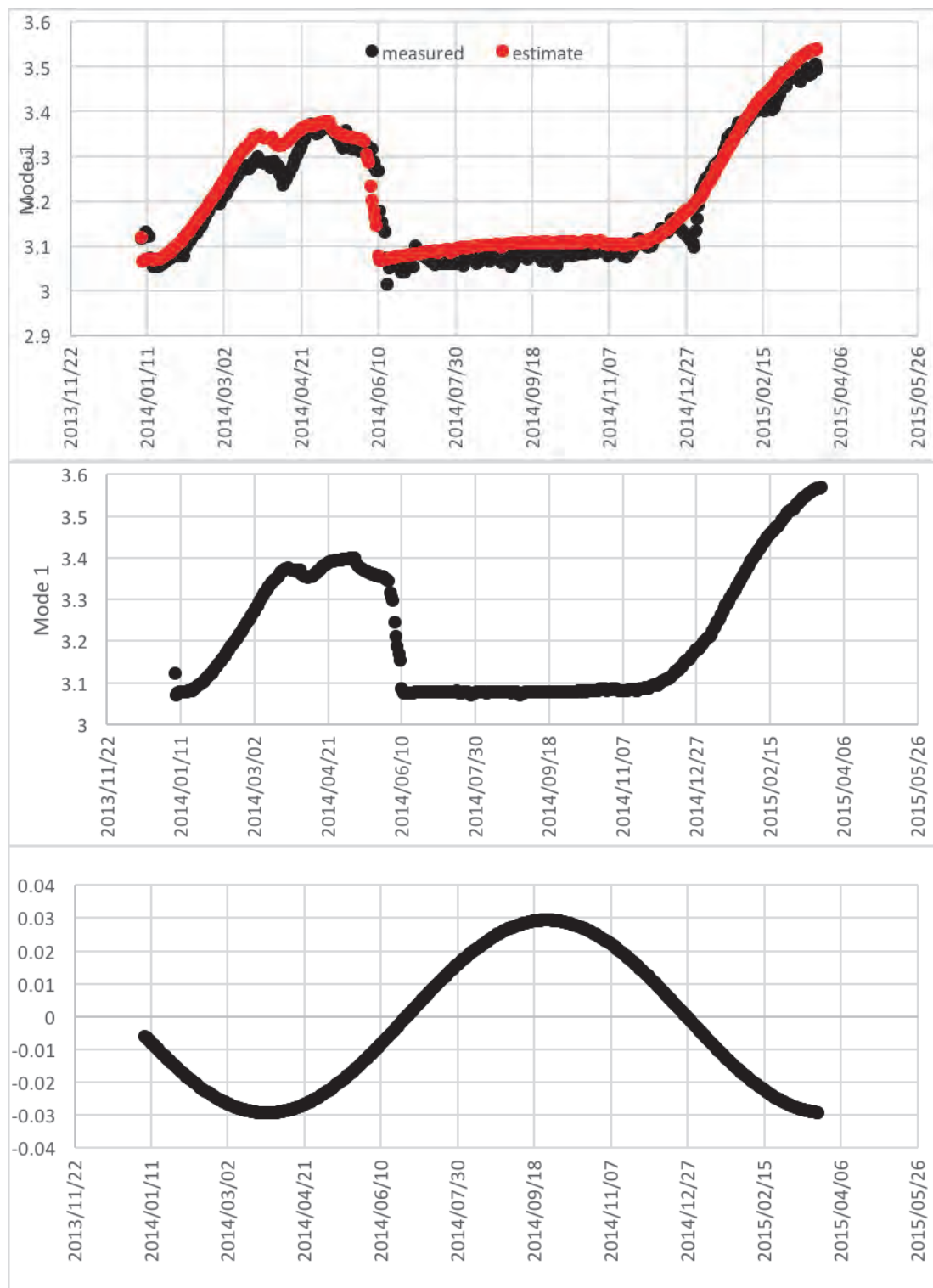


Figure 5.5: MLR-Mode 1

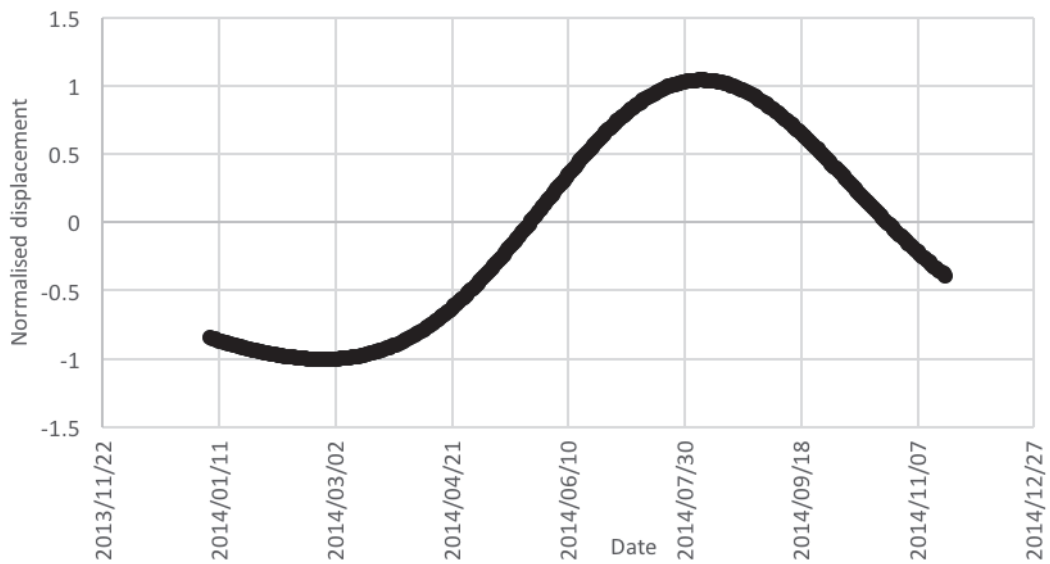
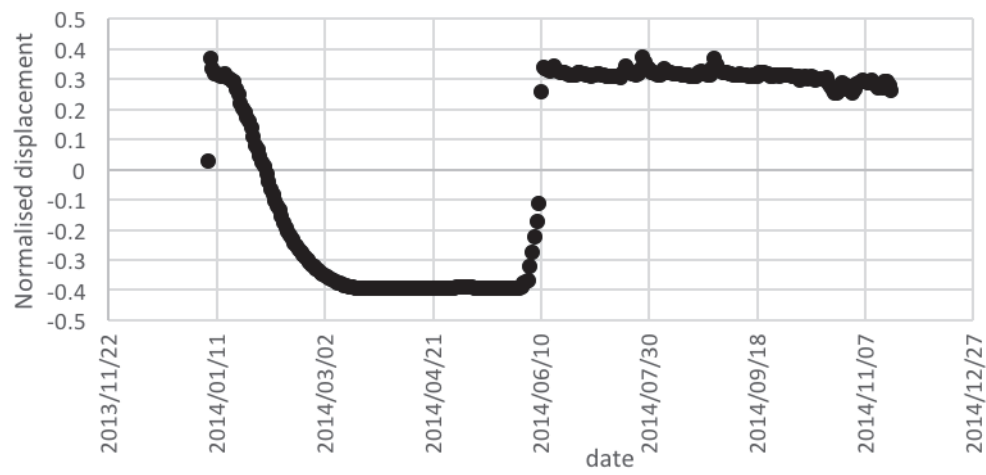
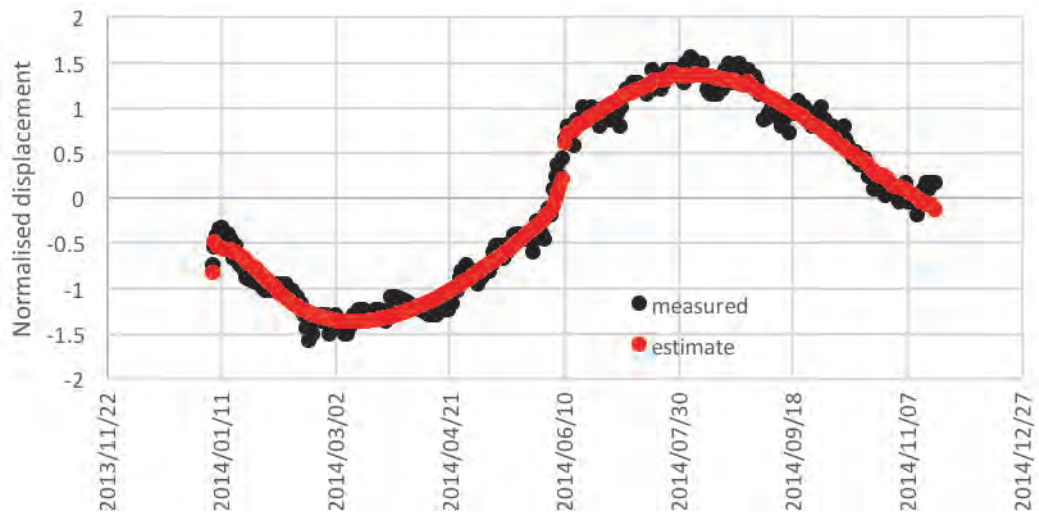


Figure 5.6: MLR-displacement

6 CONCLUSIONS & RECOMMENDATIONS

6.1 Conclusions

Dams in operation are subjected to hydrodynamic loading by the impounded water body as well as environmental loading such as temperature and wind loading. An objective of the study was to develop an updatable dynamic finite element model of the Roode Elsberg dam. Firstly, acoustic finite elements were validated as a possible formulation to represent the impounded water body. Thereafter, a parametric study was conducted, in order to ensure that all potential influences on the dynamic properties were taken into consideration. The parametric study assessed whether the divergence and the asymmetrical located reservoir had an influence on the dynamic properties under operating conditions.

The following conclusions are drawn from the study;

- (i) A 20% discrepancy was observed in the comparative study of the natural frequencies produced by the Westergaard method and FSI Model.
- (ii) The parametric study confirmed that the orientation and geometry of the reservoir have an insignificant effect on the modal parameters in the ambient state. This was attributed to the small influence the change in reservoir had on the hydrodynamic pressures exerted on the upstream surface of the dam wall. Diverging reservoir walls were found to decrease the amount of fluid excited in each mode, resulting in an increase in the natural frequencies (maximum increase of .0.8%.) An asymmetrically orientated reservoir caused an increase in the water body associated with each mode, leading to a decrease in the natural frequencies (maximum decrease of 2.5%)
- (iii) The FSI model of the Roode Elsberg dam was validated successfully using the ambient vibration measurement data, however the Westergaard method underestimated the natural frequencies by a factor of approximately 20%. With the above results, it is evident that the Westergaard method does not lead to an accurate estimation of the dynamic pressures in the ambient state. Thus, it should be only considered in preliminary studies to obtain crude estimations of the dam's dynamic properties. The acoustic fluid structure interaction method is the preferred method to be used for a more accurate idealisations of the impounded water body in the ambient state. As it provides a more realistic approach that

includes the compressibility, geometry, refraction and absorption of upstream waves and orientation of the fluid.

- (iv) The dynamic behaviour of the dam is strongly dependent on the reservoir level. The natural frequencies of the dam decrease with water level. The dam's dynamic behaviour is weakly influenced by temperature variation.
- (v) The seasonal deformation of the dam is strongly dependent on temperature variation. While the seasonal variation of deformations is largely driven by temperature variation, the reservoir level does influence the deformation of the dam especially as the dam fills rapidly.

6.2 Recommendations

To the author's knowledge, this is the first time an in-depth study comparing continuously measured dynamic properties of arch dams to continuously measured deformations. The study has shown that these parameters are critical in explaining the response of a dam to both hydrodynamic and temperature loads, and thus any anomaly detection procedure should include both to minimize false alarms. The ability to robustly discriminate the effect of environmental effects from other loads provides a powerful basis for investigating the effect of climate change on dams. It is thus recommended to use the present monitoring systems to investigate the effects of climate change on the structural performance of dams.

7 REFERENCES

1. Bathe, K. J., & Wilson, E.L. (1976). Numerical Methods in Finite Element Analysis. Prentice Hall, Englewood Cliffs, N.J., 1-582.
2. Batista et al. (2002). Models for safety control of concrete dams. In Proceedings of the 3rd International Conference on Dam Engineering (pp.1-8), Singapore.
3. Bonelli S and Poyet P (2001). Delayed response analysis of dam monitoring data, In ICOLD European symposium on Dams in a European Context (pp.91-99), Norway
4. Brincker R, & Andersen P. (2006). Understanding Stochastic Subspace Identification. *In Proceedings of the 24 International Modal Analysis Conference (IMAC)*, St. Louis, Missouri USA, 2006.
5. Alexander, M. G., & Beushausen H., (2009). Fulton's concrete technology 9th edition. *Cement & Concrete Institute*, Midrand, South Africa, 1-465
6. Chopra, K. A. (1967). Hydrodynamic pressure on dams during earthquakes. *ASCE Journal of Mechanical Engineering Division*, 205-223.
7. Chuhan, Z., Jianwen, P., & Jinting, W. (2009). Influence of seismic input mechanisms and radiation damping on arch dam response. *Soil Dynamics and Earthquake Engineering*, 1282-1293.
8. Clough, R. W. (1980) Nonlinear Mechanism in seismic response of Arch Dams. *International Conference on Earthquake Engineering*, Skopje, Yugoslavia.
9. Clough, P. W., & Tocher, J. L. (1964). Analysis of Thin Arch Dams by the Finite Element Method. *International Symposium*. Southampton: Pergamon Press, 107-122.
10. Bayraktar, A., Sevim, B., & Altunisik, C. A. (2011). Finite element model updating effects on nonlinear seismic response of arch dam-reservoir-foundation systems. *Finite elements in analysis and design*, 85-97.
11. Daniell, W. E., & Taylor, C. A. (1999). Effective ambient vibration testing for validating numerical models of concrete dams. *Earthquake engineering and structural dynamics*, 1327-1344.
12. Darbre, G. R., & Proulx, J. (2002). Continuous ambient-vibration monitoring of the arch dam of Mauvoisin. *Earthquake Engineering & Structural Dynamics*, 31(2), 475-480.
13. Dassault Systems Simulia Corp. (2010). *Abaqus/CAE User's Manual*. Providence: Dassault Systems.

14. Du, X., Zhang, Y., & Zhang, B. (2006). Nonlinear seismic response analysis of arch dam foundation systems – part I dam-foundation rock interaction. *Bulletin of Earthquake Engineering*, 5(1), 105-119.
15. Fenves, G. L., Mojtahedi, S., & Reimer, R. B. (1992). Effect of Contraction Joints on Earthquake Response of an Arch Dam. *Journal of Structural Engineering*, 118(4), 1039.
16. Fok, K. A., & Chopra, A. (1987). Water compressibility in earthquake response of arch dams. *Journal of Structural Engineering*, 958-975.
17. Fok, K. L., & Chopra, A. (1986). Earthquake analysis of arch dams including dam-water interaction, reservoir boundary absorption and foundation flexibility. *Earthquake Engineering and Structural Dynamics*, 155-184.
18. Gersdorff, N. Von. (2009). Numerical Model Validation For large Concrete Gravity Dams, 233-248.
19. Ghaemian, M., & Ghobarah, A. (1999). Nonlinear seismic response of concrete gravity dams with dam-reservoir interaction, 21, 306-315.
20. Ghanaat, Y. (1993). *Theoretical Manual for Analysis of Arch Dams*. Washington DC: U.S. Army Corps of Engineers.
21. Goldgruber, M., Shahriari, S., & Zenz, G. (2013). Influence of damping and different interaction modelling on a high arch dam, 2013(559), 28-30.
22. Housner, G. (1954). Earthquake Pressures on Fluid Containers.
23. Kuo, J. S.-H. (1982). Fluid Structure Interactions: Added Mass Computations for Incompressible Fluid. National Science Foundation.
24. Leung, A., Fok, A., Dai, H., & Su, R. (2008). The fractal finite element method for added mass type problems. *International Journal for Numerical Methods in Engineering*, 1194-1213.
25. Lew J and Loh C (2014). Structural health monitoring of an arch dam from static deformation. *Civil Structural Health Monitoring* 4,245-253.
26. Makha, R., & Moyo, P., (2012) Observations from the calibration of an arch dam model using ambient modal properties. *Concrete Repair, Rehabilitation and Retrofitting III: 3rd International Conference on Concrete Repair, Rehabilitation and Retrofitting*.
27. Mata, J. (2011). Interpretation of concrete dam's behaviour with artificial neural network and multiple linear regression models. *Engineering Structures*, 33, 903-910
28. Mivehchi, M. R., Ahmadi, M. T., & Hajmomeni, A. (2003). Effective Techniques for Arch Dam Ambient Vibration Test : Application on Two Iranian Dams, 5(2), 23-34.

29. Moyo, P., & Oosthuizen, C. (2013). *Structural Health Monitoring of Arch Dams Using Dynamic and Static Measurements*. WRC report No. K5/2025/1/13, ISBN 978-1-4312-0453-3.
30. Moyo, P., & Oosthuizen, C. (2010). Ambient Vibration Survey Trials of two arch dams in South Africa. *8th ICOLD EUROPEAN CLUB SYMPOSIUM* (pp. 589-594). Innsbruck: Grez University of Technology.
31. Nzuza, M., & Moyo, P. (2013). Thermo-Mechanical Modelling of Arch Dams for Performance Assessment. MScEng Thesis, *University of Cape Town*, 1-136.
32. Poursartip, B., & Lotfi, V. (2008). Modal Analysis of Concrete Arch Dams In Time Domain Including Dam-Reservoir Interaction.
33. Proulx, J., Darbre, G. R., & Kamileris, N. (2004). Analytical and Experimental Investigation of Damping in Arch Dams based on Recorded Earthquakes, *13th World Conference on Earthquake Engineering*, (68).
34. Rodríguez, J., Crespo, M. J., Lacoma, L. M., & Martínez, F. (2012). Fluid-Structure Interaction in Civil Engineering Structures, 1-14.
35. Samii, A., & Lofti, V. (2007). Comparison of coupled and decoupled modal approaches in seismic analysis of concrete gravity dams in time domain. *Finite Elements in Analysis and Design*, 1003-1012.
36. Sani, A. A., & Lofti, V. (2007). Linear dynamic analysis of arch dams utilizing modified efficient fluid hyper-element. *Engineering Structures*, 2654-2661.
37. Sevim, B., Bayraktar, A., & Altunisik, A. C. (2011). Journal of, (October 2010).
38. Sooch, G. S., & Bagchi, A. (2007). Effect of Seismic wave scattering on the Response of Dam-Reservoir-Foundation Systems, (1972).
39. Tiliouine, B., & Seghir, A. (1998). Fluid-structure models for dynamic studies of dam-water systems. *Eleventh European Conference on Earthquake Engineering*. Paris.
40. U.S. Army Corps of Engineers. (1994). Engineering and Design: Arch dam design. *Washington DC: Department of the Army*, 1-300.
41. United States Bureau of Reclamation. (1977). *Design of Arch Dams*. Colorado: Water Resource Technical.
42. Westergaard, H. (1933). Water Pressures on Dams During Earthquakes. *American Society of Civil Engineers*, 1(1835), 419-433.
43. Zienkiewicz, C., & Taylor, R. (2000). *The finite element method*. London: McGraw-Hill.
44. Zienkiewicz, O. C., Clough, R., & Seed, H. B. (1984). *Earthquake Analysis procedures for concrete and earth dams: State of the art*. I.C.O.L.D.